Astronomy & Astrophysics manuscript no.
(will be inserted by hand later)

UV to radio centimetric spectral energy distributions of optically-selected late-type galaxies in the Virgo cluster

A. Boselli[1], G. Gavazzi[2], and G. Sanvito[2]

[1] Laboratoire d'Astrophysique de Marseille, BP 8, Traverse du Siphon, F-13376 Marseille Cedex 12, France
e-mail: Alessandro.Boselli@oamp.fr

[2] Università degli Studi di Milano-Bicocca, Dipartimento di Fisica, Piazza dell'Ateneo Nuovo 1, 20126 Milano, Italy
e-mail: Giuseppe.Gavazzi@mib.infn.it e-mail: Gerry.Sanvito@mib.infn.it

Abstract. We present a multifrequency dataset for an optically-selected, volume-limited, complete sample of 118 late-type galaxies ($\geq$ S0a) in the Virgo cluster. The database includes UV, visible, near-IR, mid-IR, far-IR, radio continuum photometric data as well as spectroscopic data of Hα, CO and HI lines, homogeneously reduced, obtained from our own observations or compiled from the literature.
Assuming the energy balance between the absorbed stellar light and that radiated in the IR by dust, we calibarte an empirical attenuation law suitable for correcting photometric and spectroscopic data of normal galaxies. The data, corrected for internal extinction, are used to construct the spectral energy distribution (SED) of each individual galaxy, and combined to trace the median SED of galaxies in various classes of morphological type and luminosity. Low-luminosity, dwarf galaxies have on average bluer stellar continua and higher far-IR luminosities per unit galaxy mass than giant, early-type spirals. If compared to nearby starburst galaxies such as M82 and Arp 220, normal spirals have relatively similar observed stellar spectra but 10-100 times lower IR luminosities. The temperature of the cold dust component increases with the far-IR luminosity, from giant spirals to dwarf irregulars. The SED are used to separate the stellar emission from the dust emission in the mid-IR regime. We show that the contribution of the stellar emission at 6.75 μm to the total emission of galaxies is generally important, from $\sim$ 80 % in Sa to $\sim$ 20 % in Sc.

Key words. Galaxies: general – spiral – ISM – star formation

1. Introduction

An ideal tool for constraining observationally models of galaxy evolution would consist of a multi-dimensional "data-cube": $D_{imag}(\lambda, Type, Lum, z, Env)$ containing imaging data of complete samples of galaxies, spanning the broadest possible wavelength (λ), redshift (z), morphological type ($Type$) and luminosity (Lum) ranges. Moreover, all environmental conditions (Env) should be equally represented, from the coarsest "field" to the densest cluster's cores.

Such an ideal data-base is irrealistic. First of all, multifrequency images hardly exist, at suitable resolution, even for galaxies in the Local Group. The requirement that the data-cube consists of "imaging" data must then be relaxed for the more realistic requirement that it should contain "integrated" data, as more commonly available from aperture/CCD photometry. Even with these reduced characteristics, very few such data-sets exist either for high z, or for local galaxies. The presently available samples cover a small wavelength window, such as those of Connolly et al. (1995) or Kinney et al. (1993), or they are biased towards starburst and active galaxies (Schmitt et al. 1997), thus they are not representative of "normal" galaxies.

Within few years from now, however, when SLOAN will reach completion and the space missions GALEX (UV) and ASTRO-F (FIR) will perform their all-sky surveys, large data-sets meeting the above requirements will be at hands.

There is yet a sample which approaches the ideal requirements. The data-cube we are referring to is an optically selected (complete) one, representative of galaxy in a broad luminosity range and it is truly multifrequency (from the far-UV to the radio domains). It suffers from three limitations: it is local (z=0) and it represents only late-type galaxies in the densest environment, being composed of galaxies in the the Virgo cluster: $D_{phot}(UV - radio, Late, Lum, z = 0, Virgo)$. It is on this

Send offprint requests to: Alessandro Boselli

data-base that the present paper is focused.
Skipping through the details of the sample selection and of the available data that can be found in Sections 2 and 3 of this paper respectively, it is worth spending some words on what scientific purpouses such data-base is aimed at.
Individual galaxies are represented in the data-base under the form of Spectral Energy Distributions (SEDs), such as those presented in Fig. 2 (http://goldmine.mib.infn.it/papers/isosed.html). SEDs are powerful diagnostic tools for studying the energy balance between the principal constituents of galaxies. From 0.1 to 5 μm (UV, Visible, Near-IR) SEDs are dominated by the stellar thermal radiation, (but include most of the measurable recombination lines providing the diagnostics of the ISM). From 5 to 25 μm (Mid-IR) the dominant source is the radiation from very small grains of dust, but the contribution of emission lines (PAH) is relevant. From 25 to 1000 μm (Far-IR, sub-mm radio) the flux of SEDs is due to the thermal radiation from cold dust (10-100 K). Important diagnostic lines such as the [CII] ($\lambda 158 \mu m$) and CO are found in this interval. It is here that dust-rich objects peak their flux distributions. At wavelengths longer than 1 cm (radio) the radiation is non-thermal (synchrotron) by relativistic cosmic ray electrons and magnetic fields, but the most important ISM diagnostic line, the 21 cm line of the neutral hydrogen, lies in this domain. All these components and their complex feedback relations can be studied at once using the SEDs. First an estimate of the relative fraction of stars in the various age (temperature) classes can be obtained by fitting populations synthesis models (Bruzual & Charlot 1993) to the stellar continua (see e.g., Gavazzi et al. 2002a). Once the stellar populations are determined, by studying the ISM emission line properties (e.g. the Hα) one can learn about the ionization processes in HII regions. From the FIR properties we can study the dust heating mechanisms. Finally from the luminosity of the synchrotron radiation one can study the contribution of the various stellar populations to the cosmic ray acceleration.
Before energy balances can be quantitatively derived, however, the observed SEDs must be properly corrected for a number of effects that introduce wavelength dependent distortions to their shape. Primarily the SEDs must be rest-framed. Galaxies at large redshift require important K corrections. Their cosmic evolution can be studied by comparing their rest-frame SEDs with those of normal local galaxies. Hence the importance of obtaining template SEDs representative of normal galaxies, unlike those of starburst galaxies such as M82 or Arp 220 (see Fig.3), often used for such a purpouse.
Secondly comes the internal extinction correction. Stellar light is absorbed and scattered by the dust in a wavelength dependent way. Corrected SEDs can be derived if the proper amount of extinction is estimated. The amount of stellar light absorbed in the blue should equal that thermally re-emitted in the FIR by the dust. Thus the difference of the integral under the stellar continua in the SEDs before and after the extinction correction gives the energy radiated in the FIR. By reversing the argument Buat et al. (2002) derive a robust estimate of the internal extinction in normal galaxies.
Finally the comparison of SEDs of isolated and cluster galaxies can shed light on influences of the environment on the various components of galaxies. Our Virgo sample, spanning a large interval of galactocentric projected distance from M87 (up to 6 degrees), provides a clue also on this issue.
Matter in the present paper is organized as follows The sample is described in sect. (2); in sect. (3) we give a new prescription for the determination of the UV, optical and near-IR internal extinction based on the FIR/UV flux ratio. The adopted extinction law is checked in sect. (5.3) using considerations on the energy balance between the emitted far-IR radiation and the absorbed stellar light. The SEDs of the sample galaxies are presented in sect. (4), and analyzed in sect. (5). We construct template SEDs in bins of equal morphological type and luminosity and compare them to those of starburst galaxies (sect. 5.1). The stellar contribution to the mid-IR emission of galaxies (sect. 5.2) and the properties of the nonthermal radiation (sect. 5.4) are also analyzed. The bolometric properties of the observed sample are described in sect. (5.5).
New optical observations obtained using the 1.2m telescope of the Observatoire de Haute Provence (OHP), the 0.9m telescope at Kitt Peak and the 2.5m INT telescope at el Roques de los Muchachos (La Palma) are given in the appendix.
All observations analyzed in the present paper are contained in a database that has been made available to the international community via the Word Wide Web site GOLDMine (http://goldmine.mib.infn.it) described in Gavazzi et al. (2002c).

2. The sample

The sample analyzed in this work was extracted from the optically selected Virgo Cluster Catalogue (VCC) of Binggeli et al. (1985), which is complete to $B_T \leq 18$. Galaxies were selected according to the following criteria:

- $B_T < 18$
- Hubble type later than S0
- Classified as cluster member by Binggeli et al. (1985, 1993)
- lying at a projected angular distance smaller than 2 degrees from M87 (cluster-core) or greater than 4 degrees from the position of maximum projected galaxy density given by Sandage et al. (1985)(cluster- periphery), but excluding galaxies within 1.5 degrees of the M49 sub-cluster.

Table 1. Distribution of sample over Hubble type for the cluster-periphery and cluster-core subsamples.

	$S0/a-Sab$	$Sb-Sc$	$Scd-Sm$	Im	BCD
periphery	9	16	12	20	15
core	16	11	6	10	3
Total	25	27	18	30	18

– To limit the spread of distances within the sample, galaxies in the M and W clouds, and in the Southern Extension (δ(1950) <5^o) were also excluded [1].

The sky areas from which galaxies were chosen define two contrasting subsamples to optimise the statistical evaluation of the cluster environment on observed properties (see Fig. 1). The cluster-core subsample is composed of 46 galaxies within the X-ray emitting "atmosphere" of M87. The cluster-periphery subsample includes 72 galaxies in the outskirts.

The resulting sample of 118 galaxies is complete to B_T =18, and both the cluster-periphery and -core subsamples span the range -21 < M_B < -13. Both subsamples are approximately equally divided between giant spirals on the one hand and dwarf and irregular galaxies on the other. The distribution over Hubble type is summarised in Table 1.

The parameter of the sample galaxies are given in Table 2, arranged as follows:

– Column 1: VCC denomination (Binggeli et al. 1985).
– Column 2: NGC name.
– Column 3: IC name.
– Column 4: UGC name (Nilson 1973).
– Column 5: CGCG denomination (Zwicky et al. 1961-68)
– Columns 6 and 7: (B2000.0) celestial coordinates, from NED, with a few arcsec accuracy.
– Column 8: morphological type, from the VCC or from Binggeli et al. (1993).
– Column 9: photographic magnitude from the VCC.
– Columns 10 and 11: major (a) and minor (b) optical diameters (arcmin) determined at the surface brightness of 25$^{\rm th}$mag arcsec^{-2}. For galaxies without a 25$^{\rm th}$mag arcsec^{-2} value in the VCC, the diameter is computed from the "last visible" isophotal diameter given in the VCC using the relation: $Log\ a_{ext}(b_{ext}) = 0.99 Log\ a(b) + 0.1$.
– Column 12: heliocentric velocity, in km s^{-1}.
– Column 13: distance, in Mpc. Distances to the various substructures of Virgo are as given in Gavazzi et al. (1999).
– Column 14: cluster membership as defined in Gavazzi et al. (1999) [2].
– Column 15: projected angular separation from the cluster centre (M87), in degrees.
– Column 16: the model-independent near-IR concentration index parameter C_{31}, from Gavazzi et al. (2000), defined as the ratio between the radii that enclose 75% and 25% of the total light. C_{31} is a tracer of the light distribution within galaxies: values of $C_{31} < 3$ are for pure exponential discs, $C_{31} > 3$ for galaxies with bulges.
– Column 17: notes.

3. The data

The SED presented in this paper have been constructed using multifrequency data available in the literature or from our own observations, treated as consistently as possible, in order to produce an homogeneous data-set.

The UV data are taken from the FAUST (Lampton et al. 1990) and the FOCA (Milliard et al. 1991) experiments. In order to be consistent with our previous works, we transformed UV magnitudes taken at 1650 Å by Deharveng et al. (1994) to 2000 Å assuming a constant colour index UV(2000)=UV(1650)+0.2 mag. This relation has been obtained by comparing the FAUST 1650 Å with the SCAP (Donas et al. 1987) 2000 Å UV magnitudes of 17 late-type galaxies in the Virgo cluster, observed by both experiments (Deharveng et al. 1994). FOCA magnitudes are from Deharveng et al. (2002), and Donas et al., in preparation. These are total magnitudes, determined by integrating the UV emission up to the weakest detectable isophote. The estimated error on the UV magnitude is 0.3 mag in general, but it ranges from 0.2 mag for bright galaxies to 0.5 mag for weak sources observed in frames with larger than average calibration uncertainties.

U, B and V photometry is generally derived from our own CCD measurements consistently with Gavazzi & Boselli (1996), as described in the appendix. When these are not available it is derived from aperture photometry taken from the literature. The (U,B,V) D_{25} magnitudes, computed at the 25$^{\rm th}$mag arcsec^{-2} isophotal B band diameter as in Gavazzi & Boselli (1996), have $\sim$ 10 % uncertainty. They are on average 0.1 mag fainter than the total asymptotic magnitudes.

NIR data, from Nicmos3 observations, are taken mostly from Boselli et al. (1997) and Gavazzi et al. (2001). Magnitudes (J,H,K) are determined consistently with the optical magnitudes as in Gavazzi & Boselli (1996). The typical uncertainty in (J,H,K) is 10 %. As for the visible magnitudes, they are on average 0.1 mag fainter than the total asymptotic magnitudes.

[1] Some galaxies belonging to these three substructures are lying outside the regions delimited as M and W clouds and Southern Extension in Fig. 1.

[2] The Gavazzi et al. (1999) cluster membership criterion, based on the 3-D distribution of galaxies in the Virgo cluster, is slightly different from that given by Binggeli et al. (1985; 1993), used to define the sample. It is thus not surprising that several objects in Table 2 are listed as members of cluster B or of the M and W clouds.

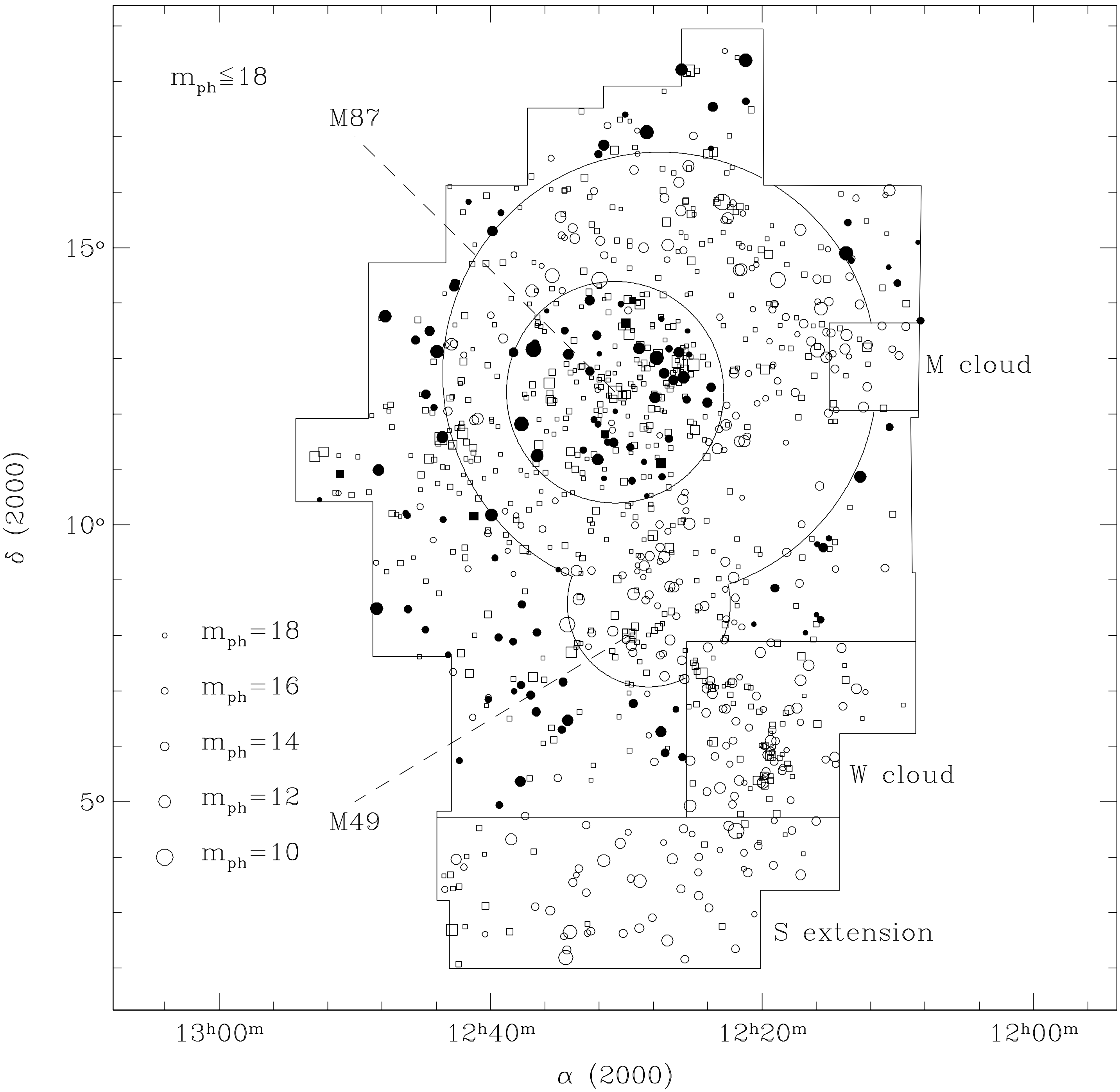

Fig. 1. Plot of all VCC galaxies classified as members by Binggeli et al. (1985) taken from figure 1 of Sandage et al. (1985). The subsample of galaxies here analyzed (see section 2) are marked with filled symbols of increasing size according to their magnitude. Empty symbols are for Virgo members not included in the ISO sample; circles for late-type galaxies (≥Sa), squares for early types (≤S0a). The 2.0 degree radius circle centred on M87 contains the cluster-core subsample. The inner boundary of the cluster periphery subsample has a radius of 4 degrees about the position of maximum projected galaxy density. The 1.5 degree radius circle is centered on the position of maximum projected galaxy density of M49 subcluster.

Mid-IR data, at 6.75 and 15 μm, are from Boselli et al. (2002c). Flux densities have been extracted from ISOCAM images by integrating the emission until the weakest detectable isophote. Even if the mid-IR emission of these galaxies is less extended than in the visible and near-IR bands, ISOCAM data provide us with integrated flux denisties representative of the whole galaxy. The typic uncertainty on the ISOCAM data is $\sim$ 30 %.

12, 25, 60 and 100 μm integrated flux densities from the IRAS survey are taken from different sources. The typical uncertainty in the IRAS data is $\sim$ 15 %. Alternative Far-IR values at 60 and 100 μm from ISOPHOT, as well as 170 μm flux densities, are taken from Tuffs et al. (2002), with a typical nominal uncertainty of $\sim$ 10 %. The comparison of ISO and IRAS data for the sample galaxies detected in both surveys reveals a systematic difference of ISO/IRAS=0.95 and 0.82 at 60 and 100 μm respectively (Tuffs et al. 2002).
We collected radio continuum data at 2.8, 6.3, 12.6 and 21 cm from different sources. 21cm radio continuum data, available for the whole sample, are mostly from the NVSS survey (Condon et al. 1998) (see Gavazzi & Boselli 1999). All radio continuum data are integrated fluxes. The typical uncertainty is $\sim$ 20 %.

The photometric data for the whole sample are given in Table 3, arranged as follows:

- Column 1: VCC denomination.
- Column 2: UV magnitude at 2000 Å, uncorrected for galactic and internal extinction.
- Columns 3-8: U, B, V, J, H, K magnitudes in the Johnson system, determined as described in Gavazzi & Boselli (1996), uncorrected for galactic and internal extinction.
- Column 9: ISOCAM 6.75 μm flux density, in mJy.
- Column 10: IRAS 12 μm flux density, in mJy.
- Column 11: ISOCAM 15 μm flux density, in mJy.
- Column 12: IRAS 25 μm flux density, in mJy.
- Column 13: IRAS 60 μm flux density, in mJy.
- Column 14: ISOPHOT 60 μm flux density, in mJy.
- Column 15: IRAS 100 μm flux density, in mJy.
- Column 16: ISOPHOT 100 μm flux density, in mJy.
- Column 17: ISOPHOT 170 μm flux density, in mJy.
- Columns 18-21: radio continuum flux densities at 2.8, 6.3, 12.6 and 21 cm, in mJy.

All data given in Table 3 are observed quantities. The UV, optical and near-IR data are uncorrected for dust extinction, the mid-IR data for the contribution of the stellar component, the radio continuum data for the contribution of the nuclear emission.

References to the photometric data are given in Table 4.

Additional emission line data are given in Table 5, arranged as follows:

- Column 1: VCC denomination.
- Column 2: Hα+[NII] equivalent width, in Å.
- Column 3: logarithm of the Hα+[NII] line, in erg cm^{-2} s^{-1}.
- Column 4: reference to the Hα data.
- Column 5: logarithm of the HI mass, in solar units, defined as $MHI = 2.36\ 10^5 D^2 SHI$, where D is the distance of the galaxy in Mpc (from Table 2), and SHI is the integrated HI flux, in Jy km s^{-1}.
- Column 6: the HI-deficiency parameter, defined as the ratio of the HI mass to the average HI mass of isolated objects of similar morphological type and linear size (Haynes & Giovanelli 1984); it is used to discriminate between "normal" galaxies and galaxies suffering for gas depletion due to ram pressure. Galaxies with an HI-deficiency parameter $\leq$ 0.3 can be treated as unperturbed, isolated galaxies.
- Column 7: the quality of the HI profile: 1 stands for high signal to noise, two-horns profiles, 2 for high signal to noise gaussian profiles, 3 for average signal to noise profiles, 4 for poor quality data and 5 for those objects whose profile is not available in the literature.
- Column 8: HI line width, measured as the average value of the width at 20 and 50 % of the peak, in km s^{-1}.
- Column 9: reference to the HI data.
- Column 10: logarithm of the H_2 mass, in solar units, defined as in Boselli et al. (2002b), determined assuming a luminosity dependent X conversion factor between the CO intensity and the H_2 surface density $logX = -0.38 logL_H + 24.23$ mol cm^{-2} (K km s^{-1})$^{-1}$.As shown in Boselli et al. (2002b), the use of a luminosity dependent rather than a metallicity dependent X conversion factor does not affect the uncertainty in the determination of the molecular hydrogen mass.
- Column 11: reference to the CO data.

Table 6. Galactic extinction law

Filter	λ	$c(\lambda)$
	Å	
UV	2000	2.10
U	3650	1.15
B	4400	1.00
V	5500	0.75
J	12500	0.21
H	16500	0.14
K'	21000	0.10

3.1. The extinction correction

UV to near-IR data have been corrected for galactic extinction according to Burstein & Heiles (1982). The galactic extinction $A_g(B)$, taken from NED and listed in Table 7, have been transformed to $A_g(\lambda)$ assuming a standard galactic extinction law (see Table 6): $A_g(\lambda)$=$c(\lambda)$ $A_g(B)$, where $c(\lambda)$=$k(\lambda)/k(B)$.

The observed stellar radiation of galaxies, from UV to near-IR wavelengths, is subject to internal extinction (absorption plus scattering) by the interstellar dust. In order to quantify the emission of the various stellar populations, UV, optical and, to a lesser amount, near-IR fluxes must be corrected for dust attenuation. Furthermore, since dust extinction varies from galaxy to galaxy (according to their geometrical parameters such as the inclination, their history of star formation and metallicity), corrections appropriate to each individual galaxy must be determined.

Estimating the dust extinction at different λ in external galaxies is however very difficult (it has been done only for the Magellanic clouds). Buat et al. (2002) have shown that, for example, the Calzetti's law calibrated on the central part of starburst galaxies (Calzetti 2001) strongly overestimates the extinction in normal, late-type objects. This difficulty is mainly due to two reasons: a) the extinction strongly depends on the relative geometry of the emitting stars and of the absorbing dust within the disc of galaxies. The young stellar population are mostly located along the disc in a thin layer, while the old populations forms a thicker layer. This point is further complicated by the fact that different dust components (very small grains, big grains etc.), which have different opacities to the UV, visible or near-IR light, have themselves different geometrical distributions both on the large and small scales. b) it is still uncertain whether the Galactic extinction law is universal, or if it changes with metallicity and/or with the UV radiation field. Detailed observations of resolved stars in the Small Magellanic Cloud by Bouchet et al. (1985) indicate that the extinction law in the optical domain is not significantly different from the Galactic one in galaxies with a UV field $\sim$ 10 times higher and a metallicity $\sim$ 10 times lower than those of the Milky Way. A steeper UV rise and a weaker 2200 Å bump than in the Galactic extinction law have been however observed in the LMC and SMC (Mathis 1990).

While the adoption of the Galactic extinction law for external galaxies seems reasonable (even though it is questionable for low-luminosity galaxies), no simple analytic functions describing the geometrical distribution of emitting stars and absorbing dust, both on small and large scales, are yet available.

The radiative transfer models of Witt & Gordon (2000) have however shown that the FIR to UV flux ratio, being mostly independent of the geometry, of the star formation history (the two radiations are produced by similar stellar populations) and of the adopted extinction law, is a robust estimator of the dust extinction at UV wavelengths. Here we will use this method to estimate the extinction correction in the UV, the wavelength most affected by dust.

We propose an internal extinction correction prescription similar to that described in Gavazzi et al. (2002a).

Our semi-empirical determination of $A(UV)$ takes into account the scattered light. Following Buat et al. (1999), we estimate $A_i(UV)$ from the relation:

$$A_i(UV) = 0.466 + Log(FIR/UV) +$$
$$+ 0.433 \times (Log(FIR/UV))^2 \qquad [\mathrm{mag}] \qquad (1)$$

where

$$FIR = 1.26 \times (2.58 \times 10^{12} \times F_{60} +$$
$$+ 10^{12} \times F_{100}) \times 10^{-26} \qquad [\mathrm{Wm^{-2}}] \qquad (2)$$

F_{60} and F_{100} are the IRAS FIR fluxes (in Jy) and

$$UV = 10^{-3} \times 2000 * 10^{(UV_{mag}+21.175)/-2.5} \qquad [\mathrm{Wm^{-2}}] \qquad (3)$$

$A_i(\lambda)$ can be derived from $A_i(UV)$ once an extinction law and a geometry for the dust and star distribution are assumed. We adopt the sandwitch model, where a thin layer of dust of thickness ζ is embedded in a thick layer of stars:

$$A_i(\lambda) = -2.5 \cdot log([\frac{1-\zeta(\lambda)}{2}](1+e^{-\tau(\lambda)\cdot sec(i)})+$$
$$+[\frac{\zeta(\lambda)}{\tau(\lambda)\cdot sec(i)}]\cdot(1-e^{-\tau(\lambda)\cdot sec(i)})) \qquad [\mathrm{mag}](4)$$

where the dust to stars scale height ratio $\zeta(\lambda)$ depends on λ (in units of Å) as:

$$\zeta(\lambda) = 1.0867 - 5.501 \cdot 10^{-5} \cdot \lambda \qquad (5)$$

Relation (5) has been calibrated adopting the average between the optically thin and optically thick cases with λ dependent dust to star scale height ratios given by Boselli & Gavazzi (1994). Observations of some edge-on nearby galaxies show that it is still unclear whether ζ depends or not on λ (Xilouris et al. 1999). As shown in Gavazzi et al. (2002a), however, similar values of $A_i(\lambda)$ are obtained in the case of a sandwitch model and of the extreme case of a slab model (ζ=1), meaning that the high uncertainty on ζ is not reflected on $A_i(\lambda)$.

In the case of the UV band (λ=2000 Å), ζ=1, and eq. (4) reduces to a simple slab model. In this case $\tau(UV)$ can be derived by inverting eq. (4):

$$\tau(UV) = [1/sec(i)] \cdot (0.0259 + 1.2002 \times A_i(UV) +$$
$$+1.5543 \times A_i(UV)^2 - 0.7409 \times A_i(UV)^3 + 0.2246 \times A_i(UV)^4) (6)$$

using the galactic extinction law $k(\lambda)$ (Savage & Mathis 1979), we than derive:

$$\tau(\lambda) = \tau(UV) \cdot k(\lambda)/k(UV) \qquad (7)$$

and we compute the complete set of $A_i(\lambda)$ using eq. (4).

FIR/UV is available for 44 objects. If FIR or UV measurements are unavailable we assume the average values $A_i(UV)$ = 1.28; 0.85; 0.68 mag for Sa-Sbc; Sc-Scd; Sd-Im-BCD galaxies respectively, as determined when FIR and UV measurements are available.

Once corrected adopting the aformentioned prescription, we checked empirically that the SED do not contain a residual dependence on galaxy inclination. The corrected SEDs of 32 Sc galaxies, binned in 4 intervals of inclination, and their fit parameters were found very consistent one another. The galactic and internal extinction correction (in magnitude) for the observed galaxies are given in Table 7.

This empirical attenuation law gives a zeroth order estimate of the attenuation in the UV regime, the most affected by dust. We stress however that the shape of the corrected spectrum, in particular at UV wavelengths, is still uncertain. This is due not only to the lack of observational constraints other than the 2000 Å flux, but also to the large uncertainties on the relative geometrical distributions of dust and stars and on the extinction law, which might significantely depend on the UV field and metallicity in this wavelength regime.

4. The SEDs

Figure 2 shows the SEDs of the sample galaxies obtained using the data given in Table 3 (only for those galaxies with at least 2 photometric data points). UV, optical and near-IR data are corrected for galactic and internal extinction as described in the previous section. FIR data at 60 and 100 μm are average values between IRAS and ISOPHOT data when both are available. When one of the two data is an upper limit, we take the detection [3]. To be as consistent as possible with IRAS, ISOPHOT data have been corrected for the average ISOPHOT/IRAS ratio found by Tuffs et al. (2002) for Virgo galaxies detected with both instruments, ISOPHOT/IRAS=0.95 and 0.82 at 60 and 100 μm respectively.

The morphological type given in Table 2 and the logarithm of the H band luminosity, defined as $logL_H = 11.36 - 0.4H_T + 2logD$ (in solar units), where H_T is the total H band magnitude and D is the distance to the source (in Mpc), are labeled in Fig. 2 (http://goldmine.mib.infn.it/papers/isosed.html). For few objects we derive the H luminosity from K band measurements assuming an average H-K colour of 0.25 mag (independent of type; see Gavazzi et al. 2000). A minority of the objects in our sample have an H band magnitude obtained from aperture photometry, thus with no asymptotic extrapolation. For these we use the H magnitude determined as in Gavazzi & Boselli (1996) at the optical radius which is on average 0.1 magnitudes fainter than H_T (Gavazzi et al. 2000).
The continuum line in the optical domain gives the integrated spectrum obtained by Gavazzi et al. (2002a). The two dashed lines at $\lambda < 10$ μm are the Bruzual & Charlot stellar population synthesis models (GISSEL 2001). The upper curves represent the models which best fit the extinction corrected data, as determined by Gavazzi et al. (2002a). The lower curves represent the same models attenuated by dust extinction using the inverse relations of sect. (3.1). For galaxies with insufficient photometric points for fitting a model, we adopt the Bruzual & Charlot model that best-fits a template SED of similar morphological type (Fig. 9 in Gavazzi et al. 2002a). To be consistent with Gavazzi et al. (2002a), all models are normalized to the V band photometric data when available, or to the K band. Given the poor quality of the fit, models are not shown for the galaxies VCC 1217 and VCC 1313.
We have preferred not to give fits in the Mid-IR range for two reasons: 1) because the very small grains and the carriers of the Aromatic Infrared Bands responsable for the mid-IR dust emission are not in thermal equilibrium with the radiation, but are stochastically heated (mostly) by UV photons (Boselli et al. 2002c). Thus modified black-body functions cannot be used to fit the mid-IR data. 2) mid-IR spectra obtained with the CVF camera onboard ISO in various galactic and extragalactic environments has shown a variety of strong emission lines with fluxes comparable with the continuum. It is thus difficult to estimate a typic mid-IR spectrum of galaxies.
The dashed line in the FIR domain (20-2000 μm) reprsents a two dust components model. Two modified blackbodies $F(\nu) \sim \nu^{\beta} B(\nu)(T_D)$, with β=2, one with a fixed warm temperature of T_w=47 K (tracing the star forming regions), the other with a (variable) cold temperature T_c (tracing the cirrus emission), were determined consistently with Popescu et al. (2002). The two components are calibrated to match the 60 and 170 μm data respectively. For galaxies not observed by PHOT but detected by IRAS at 60 and 100 μm, we adopted a modified blackbody with T_w=47 K for the warm component and we assume T_c=18 K (the average value of Popescu et al. 2002), for the cold component. They are calibrated to match the 60 and 100 μm fluxes respectively.
The far-IR to mm domain, from 170 μm to $\sim$ 1 cm, is totally unexplored. Submillimetric observation should provide constraints on the cold dust temperature and on the total dust mass of the sample galaxies. From $\sim$ 1 mm to 1 cm, data are needed to estimate the relative contribution of the thermal and synchrotron radio emission.
The dashed line in the centimetric domain, given for all galaxies with more than two detections, represents the power-law regression to the radio continuum data. The best-fit parameters are given in Table 8.

5. Analysis

Previous analyses, each devoted to a limited spectral domain, have attempted to interpret the SEDs of galaxies: Gavazzi et al. (2002a) for the continuum stellar radiation, Boselli et al. (1998, 2002c and in preparation) for the mid-IR emission, Popescu et al. (2002) for the FIR emission, and Niklas et al. (1997) for the radio emission. In this work, for the first time we analyze the SEDs as determined in the whole spectral range.

[3] The IRAS data of VCC 17 and 1725 from Almoznino & Brosch (1998) are inconsistent with the PHOT data of Tuffs et al. (2002) and with our CAM data, and are thus not used in the construction of these SEDs.

5.1. The template SED

The template SEDs in bins of morphological type and luminosity are obtained as median combinations of the normalized (to the K band) SEDs. We used only the detected values and imposed that at least 2 photometric points were available. The resulting extinction corrected template SEDs in different classes of morphological type and luminosity are shown in Fig. 3 a and c respectively. The observed (dust attenuated) SEDs of M82 and Arp220 (from Elbaz et al. 2002), are given for comparison in Fig. 3 b and d. The median values of $F(\lambda)/F(K)$ for the templates in the 18 bands considered in this work are given in Table 9, while the fitting models in the visible (corrected and uncorrected for dust extinction) and in the FIR are given in Table 10, 11 and 12 respectively [4]. The values in parenthesis in Table 9 give the total number of objects in each Hubble type and wavelength bin that were combined to form the templates.

By analyzing Fig. 3 we can observe that: a) the relative contribution to the SED of the young stellar component, emitting in the UV, and of the relatively cold dust emitting at $\sim$ 60-200 μm increases from early to late-type spirals and/or from high-mass to low-mass objects; b) the 60 to 100 μm flux density ratio increases with the total FIR emission, indicating a general increase of the big grains dust temperature from massive Sa to low-luminosity Scd-Im-BCD and, to a much higher degree, in starburst galaxies. c) optically selected spirals have UV to near-IR SEDs similar to those of sturburst galaxies such as M82 or Arp 220, despite the fact that these extreme objects have dust attenuations several order of magnitudes higher than normal galaxies, $A(UV) \sim 1$ for optically selected spirals vs. $A(UV) \sim 3.5$ for M82 (Buat et al. 2002) and $A(UV) \geq 100$ for Arp 220 (Haas et al. 2001). At the same time the far-IR emission of optically-selected, normal galaxies is more than a factor of 10-100 less important than in sturbust galaxies.

It is thus extremely dangerous to use the SEDs of starburst galaxies such as M82 and Arp 220 as templates of normal late-type galaxies at high redshift, as often done, since these objects may not be representative of the mean late-type galaxy population even at earlier epochs, when star formation was expected to be more active.

5.2. The stellar contribution to the mid-IR emission

The Bruzual & Charlot models fitted to the data trace the stellar emission from 1000 Å to 10 μm, and can thus be used to estimate the stellar contribution to the emission of our target galaxies at 6.75 μm. The ratio of the total flux (dust plus star) to the stellar flux at 6.75 μm, $[F_{6.75}(d+s)/F_{6.75}(s)]$, determined for all galaxies detected at 6.75 μm, and with available visible or near-IR photometry, is given in Table 8, while the median value for each morphological class in Table 13.

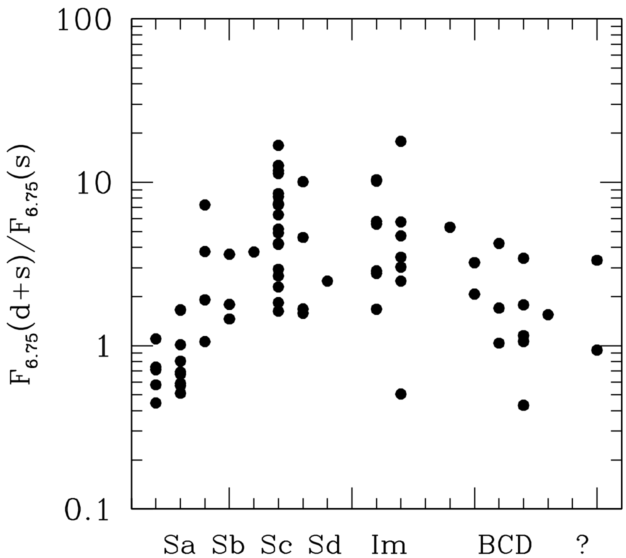

Fig. 4. The relationship between the total flux (dust plus stars) to the stellar flux at 6.75 μm, $[F_{6.75}(d+s)/F_{6.75}(s)]$, and the morphological type.

Figure 4 shows the relationship between $[F_{6.75}(d+s)/F_{6.75}(s)]$ and the morphological type. The stellar contribution to the total mid-IR emission of galaxies strongly depends on the morphological type. In early-types ($\leq$ S0a), the emission at 6.75 μm is completely dominated by the photosphere of the cold stellar population (see Table 13). The average stellar contribution to the 6.75 μm emission of spiral galaxies is always important, ranging from $\sim$ 80 % in Sa to $\sim$ 20 % to Sc and Im. In BCD the stellar emission contributes on average at $\sim$ 50 %. Given the low detection rate in irregular galaxies (Im and BCD), their average $[F_{6.75}(d+s)/F_{6.75}(s)]$ ratios might be biased towards objects whose stellar contribution to the mid-IR emission is important, the only ones with detectable 6.75 μm flux. The decrease of the dust emission observed in BCD and Im galaxies, however, could be due either to their low metallicity, or to the destruction of the carriers of the UIB expected in high UV radiation fields (Boselli et al. 1998). We do not see any strong relationship between the $[F_{6.75}(d+s)/F_{6.75}(s)]$ ratio and the total K band luminosity or concentration index parameter. However all galaxies with $C_{31}(K) > 4$ have their mid-IR emission at 6.75 μm dominated by stars. Among the ISOCAM resolved galaxies, these objects have also a $C_{31}(6.75\mu m)$ index > 4 (Boselli et al. 2002c), suggesting that the spatial distribution of the stellar component dominating the mid-IR emission is similar to that emitting in the near-IR.

In the assumption that the stars dominating the emission at $\sim$ 7 μm have a spatial distribution similar to those emitting in the near-IR, we can re-scale our K band im-

[4] A sample of Table 10 is given at the end of the paper; the whole Tables 10, 11 and 12 are available only in electronic format at http://cdsweb.u-strasbg.fr

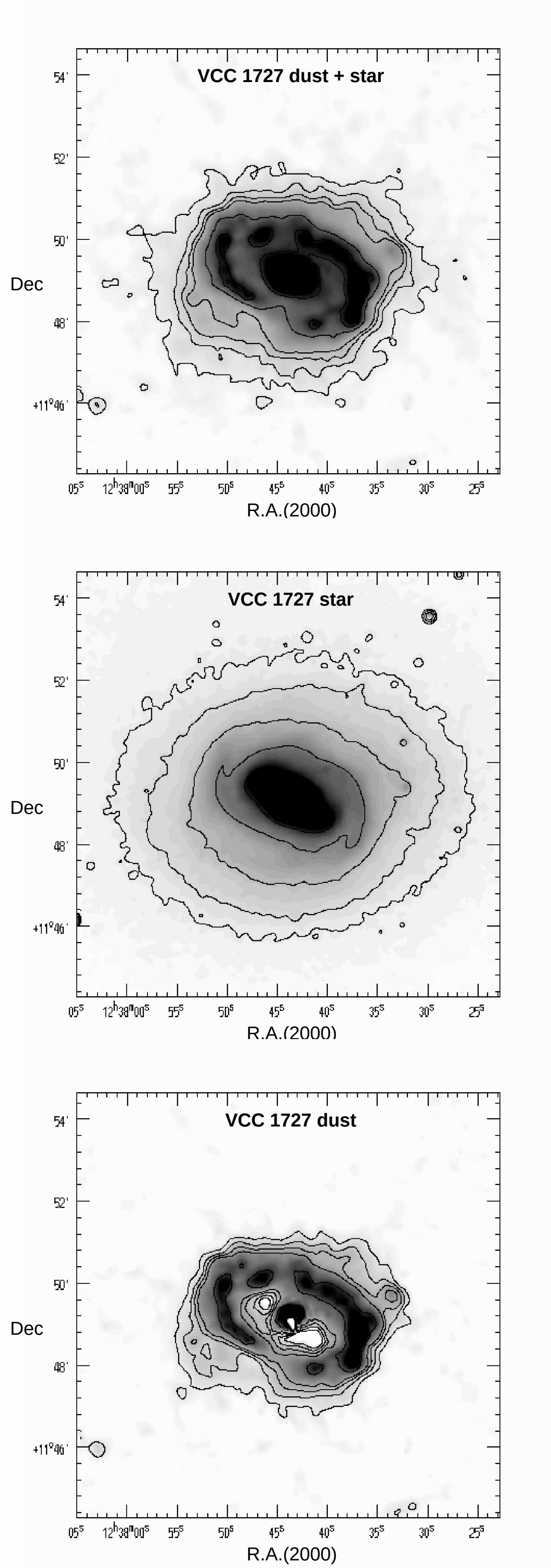

Fig. 5. The gray-level images of the Sab galaxy VCC 1727 at 6.75 μm: a) the observed images (dust+star), b) the stellar image (scaled from the K band image), c) the image of the dust emission, corrected for stellar contribution (dust). The three images are displayed with the same cuts and on the same scale (6.45 $\times$ 6.45 arcmin).

Table 13. The average stellar contribution to the 6.75 μm emission for different morphological classes

Type	$log[F_{6.75}(d+s)/F_{6.75}(s)]$
S0a	-0.17 ± 0.13
Sa-Sab	0.08 ± 0.33
Sb-Sbc	0.39 ± 0.18
Sc	0.76 ± 0.29
Scd-Sd	0.50 ± 0.30
Sm-Im	0.60 ± 0.37
BCD	0.27 ± 0.31

ages (Boselli et al. 1997) using Table 8 and subtract them from the ISOCAM LW2 images of Boselli et al. (2002c) to obtain images of the pure dust emission at 6.75 μm. We apply this correction, as an exercize to the Sab galaxy VCC 1727 (Fig. 5). The ISOCAM LW2 image at 6.75 μm shows a very pronunced nucleus, a clumpy, ring-like structure and a smoothed, diffuse external region. The emitting dust, on the contrary, is mostly located along the ring-like structure. Most of the nuclear and part of the diffuse emission in the 6.75 μm image is stellar.
The determination of the stellar contribution to the 12 and 15 μm emission of galaxies cannot be easely quantified since the Bruzual & Charlot models are limited to the spectral domain $\lambda \leq 10$ μm. The extrapolation of our fit (Fig. 2 (http://goldmine.mib.infn.it/papers/isosed.html)) indicates that the stellar contribution can be important at 15 μm, even though less than at 6.75 μm.
This result has to be taken in serious consideration when mid-IR deep surveys are used to estimate the star formation activity of galaxies at high z, where rest-frame mid-IR fluxes might be dominated by the stellar emission.

5.3. The dust emission

As extensively discussed in sect. (3.1), in a given galaxy the energy emitted by the various stellar populations and absorbed by dust must equal the total energy radiated in the mid- and far-IR domain. However $A(UV)$ was estimated in sect. (3.1) just from FIR, which is a combination of the 60 and 100 μm fluxes, not from the integral of the dust emission as determined on the SEDs. It remains to be checked whether the global extinction A(1000 Å$<\lambda<$ 10 μm), which depends on the adopted geometrical model and on the choice of the galactic extinction law, is consistent with the observed mid- and far-IR emission.

The energy of the stellar light absorbed by dust is equal to the difference between the integrals of the stellar SEDs (i.e. the Bruzual & Charlot models) prior and after the extinction correction. This should equal the energy radiated in the FIR:

$$\int_{20\mu m}^{2000\mu m} F(\lambda) d\lambda = \int_{1000\mathring{A}}^{10\mu m} F_{corr}(\lambda) d\lambda - \int_{1000\mathring{A}}^{10\mu m} F_{obs}(\lambda) d\lambda \quad (8)$$

where the integral on the left is performed under the two modified black-body functions fitted to the data between 20 and 2000 μm (far-IR). The integrals on the right are performed under the Bruzual & Charlot models prior and after the extinction correction. We disregard the dust emission in the range 5 – 20 μm due to the lack of model fitting in the mid-IR domain, whose energy contribution to the total should however be small.

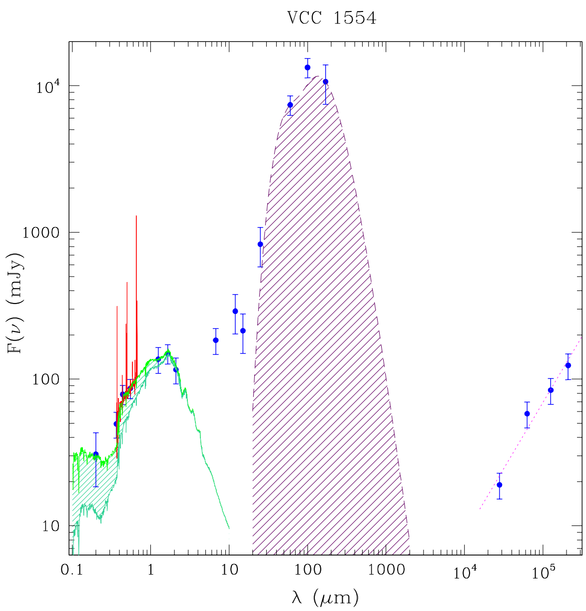

Fig. 6. The SED of the galaxy VCC 1554. The energy of the stellar light absorbed by dust is indicated by the shaded region in between the Bruzual & Chralot extinction corrected model (green continuum line) and the observed one (sky-blue continuum line) in the wavelength range 0.1-10 μm. The energy re-emitted by dust in the FIR is shown by the violet shaded region in the wavelength range 20-2000 μm. The photometric data are shown by blue dots, the optical spectrum is given in red.

To illustrate our method we give in Fig. 6 the SED of the galaxy VCC 1554. The energy of the stellar light absorbed by dust is marked by the shaded region shortward of 10 μm, the energy re-emitted in the FIR by the shaded region between 20 and 2000 μm.

Figure 7 shows the relationship between the total energy emitted in the far-IR and that emitted by stars and absorbed by dust in the range between 1000 Å and 10 μm (eq. 8). The median value of the ratio between the energy absorbed by dust and that emitted in the far-IR is 1.27 for the entire sample, 1.03 for those objects whose extinction has been determined directly using the observed FIR/UV ratio, as illustrated in Fig. 8.

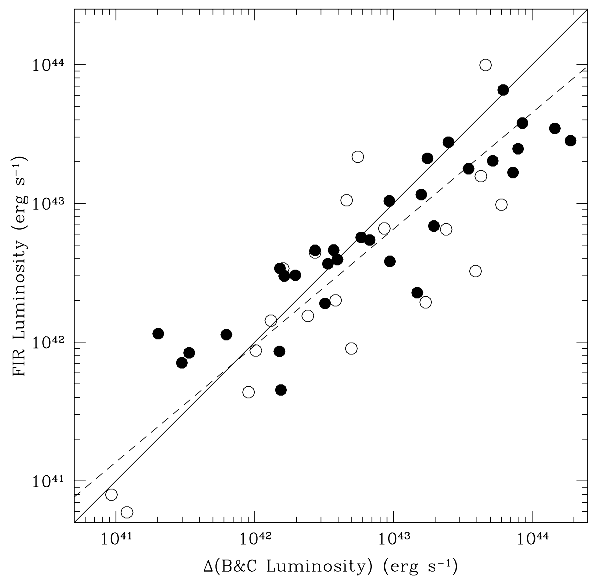

Fig. 7. The relationship between the total energy emitted in the far-IR and that emitted by stars and absorbed by dust in the range between 1000 Å and 10 μm (see eq. 8). The continuum line is the one to one relation, while the dashed line is the bysector fit. Filled symbols are galaxies whose extinction has been determined directly using the observed FIR/UV ratio, empty symbols are objects without far-IR and/or UV data, whose extinction has been determined using the average $A(UV)$ for their morphological type class.

The almost linear relation between the absorbed star light and the energy emitted by dust, combined with their ratio close to one, leads us to conclude that the prescription given in sect. (3.1) to correct stellar SEDs is sufficiently accurate for optically-selected spiral galaxies, even for objects without UV and far-IR data.

The ratio between the energy absorbed by dust and that emitted in the far-IR shows however a weak residual trend with morphological type (Fig. 9) and luminosity (Fig. 10): it is significantely larger than unity in early-type, massive galaxies.

This increase could be due to an underestimate of the far-IR emission of massive, early-type galaxies, that could exist if we missed a colder dust component in quiescent objects with low UV interstellar radiation field.

We remind that the extinction values derived using this prescription are significantly smaller than those obtained using the Calzetti's law, which is probably more accurate for starburst galaxies (see Gavazzi et al. 2002a and Buat et al. 2002 for a detailed discussion on this issue).

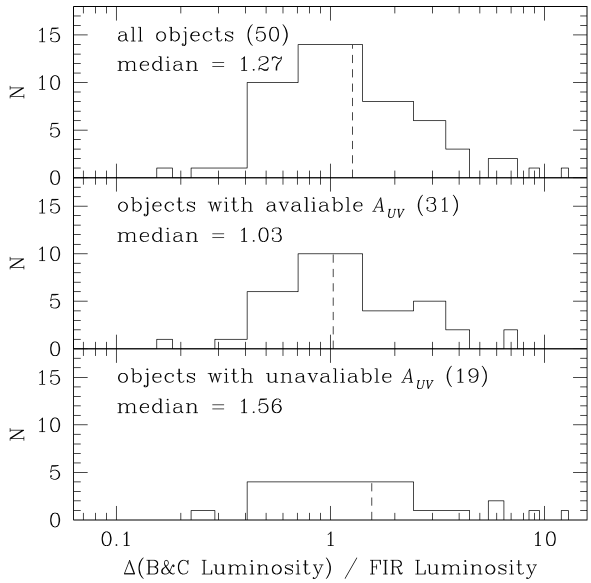

Fig. 8. The distribution of the ratio between the energy absorbed by dust and that emitted in the far-IR for the entire sample (a), for galaxies whose extinction has been determined using the observed FIR/UV ratio (b), and for those objects without far-IR and/or UV data whose extinction has been determined using the average value of $A(UV)$ for their morphological class (c).

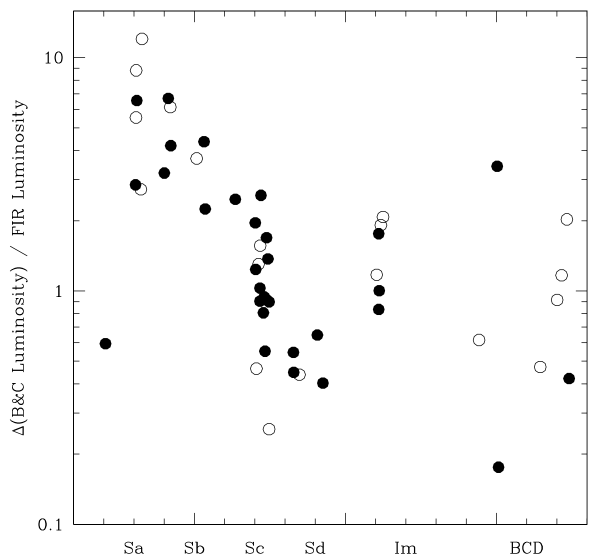

Fig. 9. The ratio between the energy absorbed by dust and that emitted in the far-IR as a function of the morphological type. Symbols as in Fig. 7.

5.4. The radio emission

For 25 galaxies detected at more than one frequency in the centimetric domain, we derive the slope of the radio continuum spectrum by a simple linear fit to the data. Excluding galaxies VCC 857, 1110 and 1450 showing large inconsistencies in the radio continuum flux densities and 8 additional objects with signs of nuclear activity (LINER, Seyfert, see Table 2) we obtain an average spectral slope α=0.76 $\pm$ 0.27, consistent with the canonical synchrotron slope α=0.8 found by Niklas et al. (1997) by carefully separating the contribution of the thermal from the synchrotron emission (see Table 8).

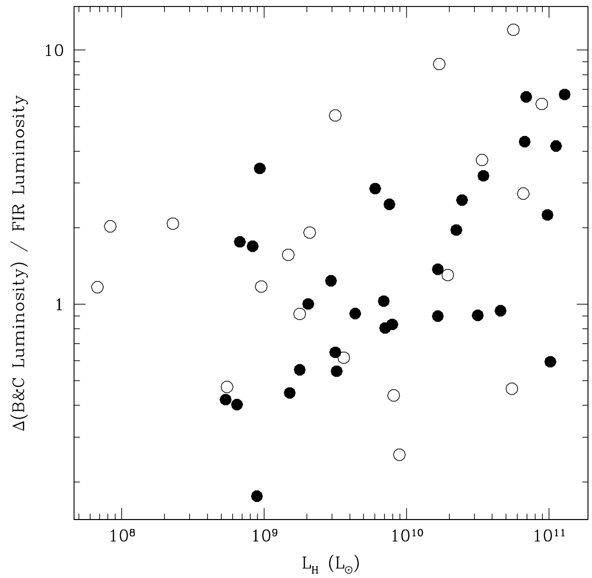

Fig. 10. The ratio between the energy absorbed by dust and that emitted in the far-IR as a function of the H band luminosity. Symbols as in Fig. 7.

5.5. The bolometric luminosity of optically-selected, late-type galaxies

By integrating the fit models in the stellar and FIR domain, we calculate the (observed) bolometric luminosity of our target galaxies:

$$L_{Bol} = \int_{1000\mathring{A}}^{10\mu m} F_{obs}(\lambda) d\lambda + \int_{20\mu m}^{2000\mu m} F(\lambda) d\lambda \qquad (9)$$

As before, we disregard the contribution of UIB and of the very small grains in the 5-50 μm range, thus this esitimate gives a lower limits to the total bolometric luminosity.
Figure 11 shows that the bolometric luminosity of optically-selected late-type galaxies in the range $10^8 \leq L_{bol} \leq 10^{11}$ L$\odot$, is dominated by the stellar emission. The median value of the ratio between the energy emitted by stars in the 1000 Å- 10 μm range and by dust in the Far-IR is 4.0, significantly higher than $f_B/f_{FIR} \sim 1.6$ found by Soifer et al. (1987) who determined the stellar emission from the B band luminosity alone. No relation is observed between the stellar to FIR ratio and the bolometric luminosity, except for an higher dispersion at high luminosity.

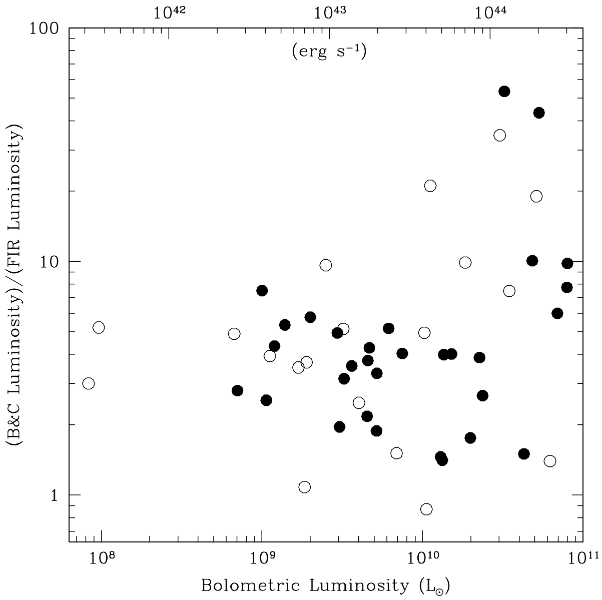

Fig. 11. The relationship of the ratio of the total uncorrected stellar luminosity (from the Bruzual & Charlot model) to the total FIR luminosity versus the bolometric luminosity of the target galaxies. Symbols are as in Fig. 7.

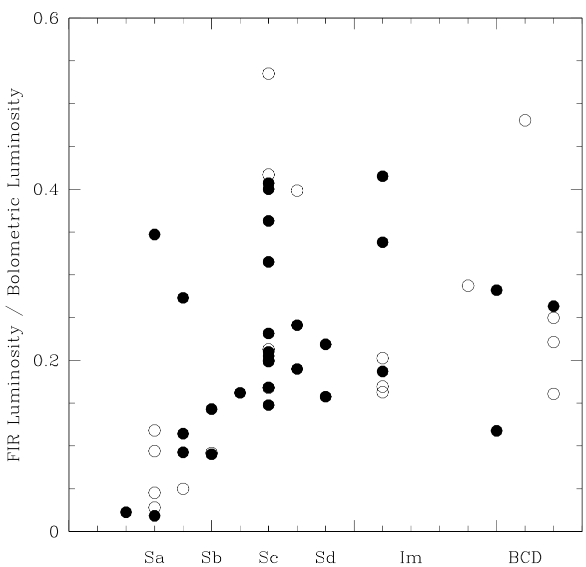

Fig. 12. The relationship between the far-IR to bolometric luminosity ratio and the morphological type. Symbols are as in Fig. 7.

Figure 12 shows that the far-IR to bolometric luminosity ratio increases from early Sa spirals ($L_{FIR}/L_{bol} \leq 0.1$) to Sc-Sd galaxies ($L_{FIR}/L_{bol} \sim 0.2 - 0.4$), consistently with Popescu & Tuffs (2002). BCDs have values of $L_{FIR}/L_{bol} \sim 0.2$, significantly lower than those estimated by Popescu & Tuffs (2002) ($L_{FIR}/L_{bol} > 0.5$). This discrepancy is probably due to a different determination of the stellar contribution to the bolometric luminosity. Our complete and homogeneous dataset allowed a more accurate determination of the total stellar emission than in Popescu & Tuffs (2002), in particular for BCD galaxies where the contribution of the UV emission, here determined for several objects using unpublished UV data, might be dominant.

6. Summary and Conclusions

We present a multifrequency dataset comprising an optically-selected, volume-limited, complete sample of 118 galaxies in the Virgo cluster. The sample includes all late-type (≥ S0a) Virgo A members in the core of the cluster, with projected distance $\Theta < 2$ degrees from M87, or at the peryphery of the cluster ($\Theta > 4$ degrees from the position of maximum projected galaxy density).

The database includes UV, visible, near-IR, mid-IR, far-IR, radio continuum photometric data as well as spectroscopic data on the Hα, CO and HI lines.

Spectral energy distributions (SEDs) of the individual galaxies, as well as templates SEDs in bins of morphological type and luminosity are derived. The SEDs are fitted with stellar population synthesis models providing an estimate of the total stellar radiation, with modified black-bodies fitted to the far-IR data giving the energy re-emitted by dust, and with power laws representing the synchrotron emission.

Assuming the energy balance between the absorbed stellar light and the energy radiated in the IR by dust, we calibrate an empirical attenuation law suitable for correcting photometric and spectroscopic data of normal galaxies.

The analysis of the SED show that low-luminosity, dwarf galaxies have on average bluer stellar continua and higher far-IR luminosities (per unit galaxy mass) than giant, early-type spirals. Normal spirals have relatively similar observed stellar spectra but 10 to 100 times lower IR luminosities than nearby starburst galaxies such as M82 and Arp 220. The temperature of the cold dust component increases with the far-IR luminosity, from giant spirals to dwarf irregulars and to an higher extent in starburst galaxies. SEDs of starburst galaxies should not be used as templates of normal high redshift galaxies. We show that the contribution of the stellar emission to the 6.75 μm mid-IR flux is generally important, from ∼ 80 % in Sa to ∼ 20 % in Sc.

Acknowledgements. We thank J. Donas and D. Pierini for providing us with unpublished UV and near-IR data. We thank S. Arnouts, V. Buat and M. Sauvage for stimulating discussions, and D. Elbaz for providing us with the SED of M82 and Arp 220. This research has made use of the NASA/IPAC Extragalactic Database (NED) which is operated by the Jet Propulsion Laboratory, California Institute of Technology, under contract with the National Aeronautics and Space Administration. most of the data presented in this work are available through the WEB page http://goldmine.mib.infn.it.

References

Almoznino E., Brosch N., 1998, MNRAS, 298, 920
Binggeli B., Sandage A., Tammann G., 1985, AJ, 90, 1681 (VCC)
Binggeli B., Popescu C., Tammann G., 1993, A&AS, 98, 275
Boselli A., Gavazzi G., 1994, A&A, 283, 12
Boselli A., Gavazzi G., 2002, A&A, 2002, 386, 124
Boselli A., Casoli F., Lequeux J., 1995, A&AS, 110, 521
Boselli A., Tuffs R., Gavazzi G., Hippelein H., Pierini D., 1997, A&A 121, 507
Boselli A., Lequeux J., Sauvage M., 1998, et al. A&A 335, 53
Boselli A., Iglesias-Paramo J., Vilchez J., Gavazzi G., 2002a, A&A, 2002, 386, 134
Boselli A., Lequeux J., Gavazzi G., 2002b, A&A, 384, 33
Boselli A., Sauvage M., Lequeux J., Donati A., Gavazzi G., 2002c, A&A, in press
Bothun G., Mould J., Caldwell N., Mac Gillivray H., 1986, AJ, 92, 1007
Bottinelli L., Gouguenheim L., Fouque P., Paturel G., 1990, A&AS, 82, 391
Bouchet P., Lequeux J., Maurice E., Prevot L., Prevot-Burnichon M., 1985, A&A, 149, 330
Bruzual G., Charlot S., 1993, ApJ, 405, 538
Buat V., Donas J., Milliard B., Xu C., 1999, A&A, 352, 371
Buat V., Boselli A., Gavazzi G., Bonfanti C., 2002, A&A, 383, 801
Bursetin D., Heiles C., 1982, AJ, 87, 1165
Bursetin D., Davies R., Dressler A., et al., 1987, ApJS, 64, 601
Calzetti D., 2001, PASP, 113, 1449
Combes F., Dupraz C., Casoli F., Pagani L., 1988, A&A, 203, L9
Condon J., 1987, ApJS, 65, 485
Condon J., Helou G., Sanders D., Soifer B., 1990, ApJS, 73, 359
Condon J., Cotton W., Greisen E., et al., 1998, AJ, 115, 1693 (NVSS)
Connolly A., Szalay A., Bershady M., Kinney A., Calzetti D., 1995, AJ, 110, 1071
Deharveng J.M., Sasseen T., Buat V., Bowyer S., Lampton M., Wu X., 1994, A&A, 289, 715 (FAUST)
Deharveng J.M., Boselli A., Donas J., 2002, A&A, in press
de Vaucouleurs G., de Vaucouleurs A., Buta R., 1981, AJ, 86, 1429
Donas J., Deharveng J.M., Laget M., Milliard B., Huguenin D., 1987, A&A, 180, 12
Dressel L., Condon J., 1978, ApJS, 36, 53
Elbaz, D., Cesarsky, C. J., Chanial, P., et al., 2002, A&A, 384, 848
Frueh M.L., Corwin H.G., de Vaucouleurs G., Buta R., 1996, AJ, 111, 722
Gallagher J., Hunter D., 1986, AJ, 92, 557
Gavazzi G., Boselli A., 1996, Astro. Lett. and Communications, 35, 1
Gavazzi G., Boselli A., 1999, A&A, 343, 86
Gavazzi G., Garilli B., Carrasco L., Boselli A., Cruz-Gonzalez I., 1994, A&AS, 104, 271
Gavazzi G., Boselli A., Carrasco, L., 1995, A&AS, 112, 257
Gavazzi G., Boselli A., Scodeggio M., Pierini D., Belsole E., 1999, MNRAS, 304, 595
Gavazzi G., Franzetti P., Scodeggio M., Boselli A., Pierini D., 2000, A&A, 361, 863
Gavazzi G., Zibetti S., Boselli A., Franzetti P., Scodeggio M., Martocchi S., 2001, A&A, 372, 29
Gavazzi G., Bonfanti C., Sanvito G., Boselli A., Scodeggio M., 2002a, ApJ, 576, 135
Gavazzi G., Boselli A., Pedotti P., Gallazzi A., Carrasco L., 2002b, A&A, 386, 114
Gavazzi G., Boselli A., Donati A., Franzetti P., Scodeggio M., 2002c, A&A, in press
Giovanardi C., Krumm N., Salpeter E., 1983, AJ, 88, 1719
Haas M., Klaas U., Müller S., Chini R., Coulson I, 2001, A&A, 367, L9
Haynes M., Giovanelli R., 1984, AJ, 89, 758
Haynes M., Giovanelli R., 1986, ApJ, 306, 466
Heller A., Almoznino E., Brosch N., 1999, MNRAS, 304, 8
Helou G., Salpeter E., Giovanardi C., Krumm N., 1981, ApJS, 46, 267
Helou G., Salpeter E., Terzian Y., 1982, AJ, 87, 1443
Helou G., Hoffman G., Salpeter E., 1984, ApJS, 55, 433
Helou G., Khan I., Malek L, Boehmer L., 1988, ApJS, 68, 151
Hoffman L., Helou G., Salpeter E., Glosson J., Sandage A., 1987, ApJS, 63, 247
Hoffman L., Williams H., Salpeter E., Sandage A., Binggeli B., 1989a, ApJS, 71, 701
Hoffman G., Lewis B., Helou G., Salpeter E., Williams B., 1989b, ApJS, 69, 65
Huchtmeier W., Richter O., Bohnenstengel H., Hauschildt M., 1989, A General Catalogue Of Hi Observations Of External Galaxies, New York, Springer-Verlag
Kenney J., and Young J., 1988, ApJS, 66, 261
Kinney A., Bohlin R., Calzetti D., Panagia N., Wyse R., 1993, ApJS, 86, 5
Koopmann R., Kenney J., Young J., 2001, ApJS, 135, 125
Kotanyi C., 1980, A&AS, 41, 421
Isobe T., Feigelson E., 1992, ApJS, 79, 197
Lampton M., Deharveng J.M., Bowyer S., 1990, in IAU Symposium 139, The Extragalatic Background Radiation, ed. S. Bowyer & C. Leinert (Dordrecht: Kluwer), p449
Landolt A., 1983, AJ, 88, 439
Longo G., de Vaucouleurs A., Corwin H., 1983, "A Catalogue of Photoelectric Magnitudes and Colors in the UBV System of 3578 Galaxies Brighter than 16th V Magnitude (1936-1982)", University of Texas, Austin
Longo G., de Vaucouleurs A., 1985, "A General Catalogue of Photoelectric Magnitudes and Colors of Galaxies in the UBV System - Supplement", University of Texas, Austin
Lonsdale C., Helou G., Good J., Rice W., 1985, in "Catalogued galaxies and quasars observed in the IRAS survey",JET Propulsion Laboratory
Magri C., 1994, AJ, 108, 896
Mathis J., 1990, ARA&A, 28, 37
Milliard B., Donas J., Laget M., 1991, Advances in Space Research, Vol. 11, 135
Niklas S., Klein U., Wielebinski R., 1995, A&A, 293, 56
Niklas S., Klein U., Wielebinski R., 1997, A&A, 322, 19
Nilson, P., 1973, *Uppsala General Catalogue of Galaxies*, (Uppsala Obser. Annu. Vol. 6) (UGC)
Popescu C., Tuffs R., 2002, MNRAS, in press (astroph/0208285)
Popescu C., Tuffs R., Völk H., Pierini D., Madore B., 2002, ApJ, 567, 221
Prugniel P., Heraudeau P., 1998, A&AS, 128, 299
Rush B., Malkan M., Spinoglio L., 1993, ApJS, 89, 1
Sage L., Wrobel J., 1989, ApJ, 344, 204
Sandage, A., Binggeli, B., & Tammann, G.A., 1985, AJ, 90, 1759

Savage B., Mathis J., 1979, ARA&A, 17, 73
Schmitt H., Kinney A., Calzetti D., Storchi Bergmann T., 1997, AJ, 114, 592
Schneider S., Thuan T., Magri C., Wadiak J., 1990 ApJS, 72, 245
Schroeder A., Visvanathan N., 1996, A&AS, 118, 441
Soifer B., Sanders D., Madore B., et al., 1987, ApJ, 320, 238
Soifer B., Boehmer L., Neugebauer G., Sanders D., 1989, AJ, 98, 766
Stark A., Knapp G., Bally J., Wilson R., Penzias A., Rowe H., 1986, ApJ, 310, 660
Takamiya M., Kron R.G., Kron, G.E. 1995, AJ 110, 1083
Thuan T., Sauvage M., 1992, A&AS, 92, 749
Tuffs R., Popescu C., Pierini D., et al., 2002, ApJS, 139, 37
Warmels R., 1986, Ph.d. Thesis
Witt A.N., Gordon K.D., 2000, ApJ, 528, 799
Xilouris E., Byun Y., Kylafis N., Paleologou E., Papamastorakis J., 1999, A&A, 344, 868
Young J., Allen L., Kenney J., Lesser A., Rownd B., 1996, AJ, 112, 1903
Zwicky F., Herzog E., Karpowicz M., Kowal C., Wild P., 1961-1968, "Catalogue of Galaxies and of Cluster of Galaxies" (Pasadena, California Institute of Technology; CGCG)

Appendix: UBV CCD photometry of Virgo galaxies [5]

The present work is partly based on new CCD optical photometry of 36 galaxies obtained at the 1.20m Newton telescope at the Observatoire d'Haute Provance (OHP, France), at the 0.9m telescope at Kitt Peak and at the 2.5m INT telescope at La Palma. The OHP and the INT observations were taken during the Hα surveys presented in Boselli & Gavazzi (2002) and Boselli et al. (2002a) respectively. Details on the observations and data reduction procedures are found in these papers. Kitt Peak targets were observed as fillers during an Hα survey of isolated galaxies.

The $f/6$ 1.2m OHP telescope was equipped with a thinned TK1024×1024 pixels CCD detector, with a pixel size of 0.69 arcsec and a field of view of 11.8×11.8 arcminuts. At the adopted gain, the electron/adu conversion is 3.5 e^{-}/adu, with a readout noise of 8.5 e^{-}. Thirty galaxies of the present sample were observed during 26 nights in two runs, in 1998 and 2000. Fourteen galaxies were imaged in the V, 30 in the B and 1 in the U band. The observations were done in poor seeing conditions, ranging from 2 to 4 arcsec. The typical integration time was 10 minuts in the V, 15 in the B and 30 in the U bands.

INT B band imaging of 2 galaxies were obtained in 1999 using the Wide Field Camera (WFC) attached at the prime focus of the $f/3.29$ 2.5m telescope. The WFC is composed by a science array of four thinned AR coated EEV 4K×2K CCDs, plus a fifth acting as autoguider. The pixel scale at the detectors is 0.33 arcsec pixel^{-1}, which gives a total field of view of about 34×34 arcmin^2. The observations were done during photometric conditions, with an average seeing of 1.5-2 arcsec and an integration time of 10 minutes.

Kitt Peak B band imaging of 5 galaxies were obtained during 4 nights in 1995 using the 0.9m telescope in the $f/13$ configuration, equipped with a T2KA 2048×2048 pixel CCD, with a pixel size of 0.384 arcsec pixel^{-1} and a total field of view of 13.1×13.1 arcminuts. At the adopted gain, the electron/adu conversion is 2 e^{-}/adu, with a lecture noise of 4 e^{-}. The observations were done during non photometric conditions, with an average seeing of 1-1.5 arcsec and an integration time of 15 minutes.

[5] The Observatoire de Haute Provence (OHP) (France), is operated by the French CNRS; the INT telescope is operated on the island of La Palma by the ING team in the Spanish Observatorio del Roque de Los Muchachos of the Instituto de Astrofsica de Canarias; KPNO is operated by AURA, Inc. under contract to the National Science Foundation.

The observations were calibrated and transformed into the Johnson UBV system using standard stars in the catalogue of Landolt (1983). Observations of the standard stars were repeated every 2 hours. Repeated measurements gave < 0.10 mag differences, which we assume as the typical uncertainty of the photometric result given in this work. Not all frames were obtained in photometric conditions. When the zero point was varing by more than 0.05 mag due to cirrus, we choose to observe only galaxies with available multiaperture photometry in order to perform the calibration a posteriori.

The data reduction of the CCD images follows a procedure identical to the one described in previous papers of the series (Gavazzi et al. 1995), based on the IRAF STSDAS data reduction packages. To remove the detector response each image is bias subtracted and devided by the mean of 5 flat field exposures obtained on the twilight sky. Direct inspection of the frames allows manual cosmic rays removal and subtraction of contaminating objects, such as nearby stars and galaxies. The sky background is determined in each frame in concentric object-free annuli around the object. The typical uncertainty on the mean background is estimated 10 % of the rms in the individual pixels. This represents the dominant source of error in low S/N regions. The determination of object centroid is performed by fitting gaussian two-dimensional profiles to the data, centered on the brightest excess in each object, generally corresponding to the nucleus. At the central coordinates determined, a growth curve is derived for each object by integrating the counts in concentric circular rings of increasing radii. The obtained growth curves, transformed from counts to magnitudes, are then compared with the multiaperture photometry available in the literature, in order to check our photometric calibration and to obtain a zero point for those objects observed in non-photometric conditions. At this stage stars projected within the target galaxies were not subtracted since, unless specified, reference aperture photometry usually includes them. Once the accurate zero point is obtained for each galaxy, a similar procedure is repeated after subtracting contaminating stars and galaxies. Following the procedure described in Gavazzi & Boselli (1996), a magnitude is obtained after integrating along circular, concentric annuli up to the isophotal 25 mag arcsec^{-2} B diameter. To improve the photometric accuracy, this procedure is applyed adding our measurements with aperture photometry available in the literature. UBV magnitudes of the target galaxies are given in Table 3. The estimated error on the magnitude is ~ 10 %.

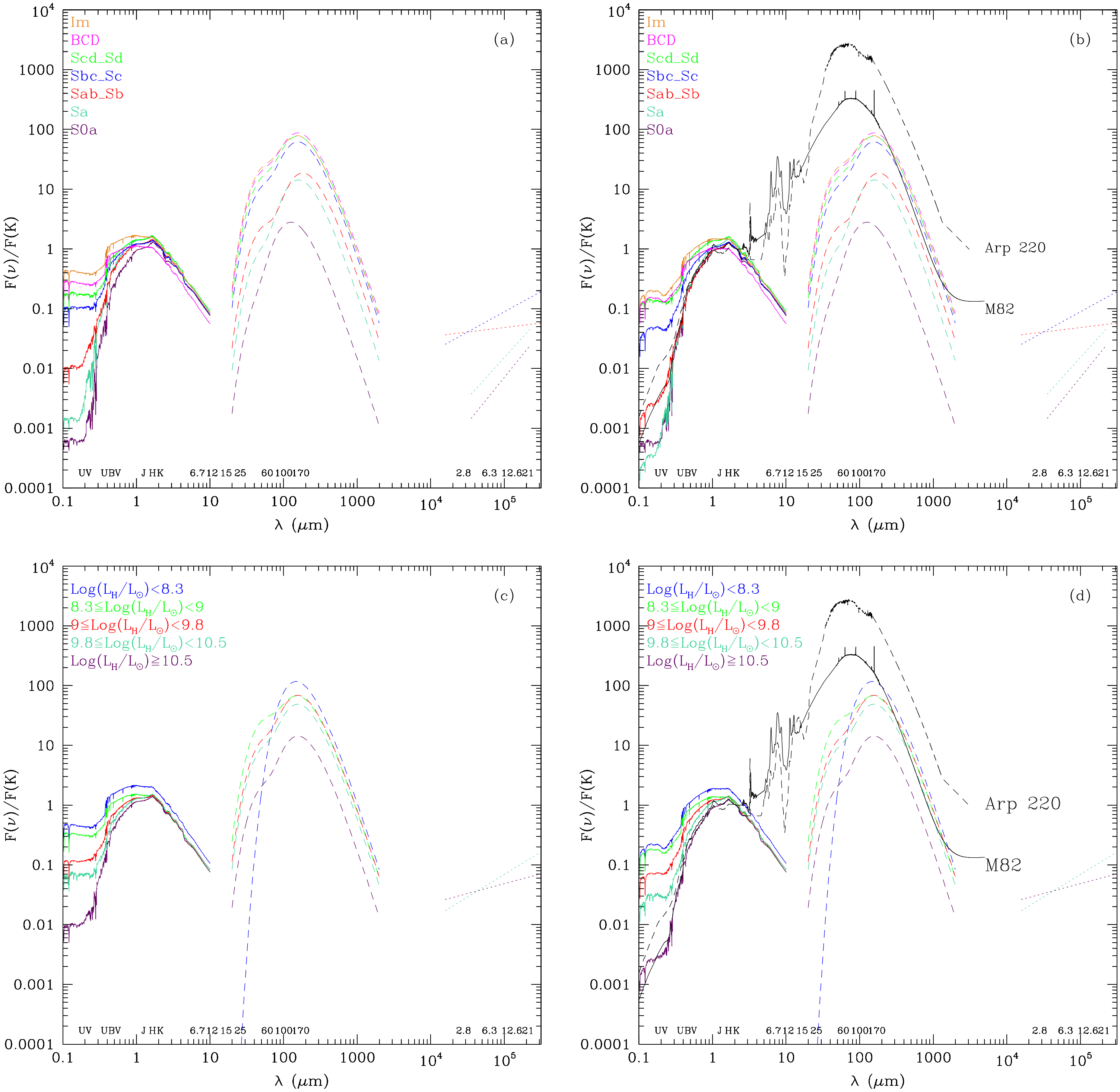

Fig. 3. The extinction corrected (a) and dust attenuated (b) template SEDs in bins of morphological type and luminosity (c,d). The dust attenuated SEDs of M82 (continuum black line) and Arp 220 (dotted black line) are also given for comparison.

Table 2: The target galaxies

VCC	NGC	IC	UGC	CGCG	R.A.(2000)	dec	type	m_{pg}	a	b	vel	$Dist$	memb.	θ	C_{31}	com
					h m s	° ′ ″		mag	′	′	km s^{-1}	Mpc		deg		
(1)	(2)	(3)	(4)	(5)	(6)	(7)	(8)	(9)	(10)	(11)	(12)	(13)	(14)	(15)	(16)	(17)
1	-	-	-	69059	120820.02	134100.2	BCD?	14.78	0.80	0.18	2267	32	M	5.63	3.36	
4	-	-	-	-	120830.75	150548.2	Im	17.50	0.50	0.43	589	32	M	6.06	-	
17	-	3023	7150	-	121001.86	142142.4	Im	15.20	0.91	0.45	819	32	M	5.43	2.85	
24	-	-	-	69070	121035.65	114538.5	BCD	14.95	1.00	0.37	1289	32	M	4.99	6.23	
26	-	-	-	-	121040.20	143848.5	Im	17.50	0.43	0.27	2469	32	M	5.39	2.35	
66	4178	-	7215	69088	121246.27	105156.0	SBc(s)	11.89	5.35	1.87	369	17	N	4.68	3.24	*
81	4186	-	7223	-	121326.18	144620.1	d:Sc	15.60	0.95	0.81	2075	17	N	4.85	3.22	
87	-	-	-	98106	121340.91	152713.2	Sm	15.00	1.45	0.72	-134	17	N	5.17	3.18	
92	4192	-	7231	98108	121348.24	145401.2	Sb:	10.92	9.78	2.60	-135	17	N	4.84	5.04	*
130	-	-	-	-	121504.22	94513.5	BCD	16.50	0.63	0.25	2189	17	N	4.68	2.71	
152	4207	-	7268	69107	121530.31	93508.6	Scd(on edge)	13.48	1.96	0.89	592	17	N	4.69	3.54	
159	-	-	-	69108	121541.50	81707.7	Im	15.08	1.04	0.52	2584	32	W	5.54	2.73	
169	-	-	-	-	121556.39	93855.7	Im	16.50	0.85	0.43	2222	17	N	4.57	-	
171	-	-	-	-	121558.88	82225.8	Im	17.40	0.57	0.36	875	32	W	5.43	-	
207	-	-	-	-	121648.07	80302.0	BCD	17.20	0.36	0.13	2564	32	W	5.55	2.63	
318	-	776	7352	70005	121903.40	85122.7	SBcd	14.01	1.71	1.00	2469	32	W	4.57	2.93	
425	-	-	-	-	122035.90	81209.3	Im:	17.30	0.43	0.38	-	23	B	4.89	-	
459	-	-	-	99022	122111.46	173818.5	BCD	14.95	0.84	0.36	2108	17	A	5.74	3.09	
460	4293	-	7405	99023	122112.68	182256.5	Sa pec	11.20	5.10	2.92	921	17	A	6.42	3.52	*
655	4344	-	7468	99037	122337.45	173228.5	S pec,N:/BCD	13.21	1.55	1.55	1147	17	A	5.44	2.50	
664	-	3258	7470	70042	122344.36	122842.5	Sc	13.50	2.60	1.87	-427	17	A	1.73	2.55	
666	-	-	-	-	122346.13	164728.5	Im:	16.80	1.00	0.57	-	17	A	4.72	2.80	
692	4351	-	7476	70045	122401.37	121216.6	Sc(s)	12.93	2.92	1.87	2324	17	A	1.67	2.95	
793	-	-	-	-	122521.88	130423.2	Im,N?	16.74	0.47	0.34	1906	17	A	1.50	2.25	
802	-	-	-	-	122529.01	132947.3	BCD	17.40	0.64	0.21	-215	17	A	1.71	2.58	
809	-	3311	7510	70063	122533.17	121536.3	Sc (on edge)	14.55	1.45	0.36	-142	17	A	1.30	3.24	
836	4388	-	7520	70068	122546.60	123940.4	Sab	11.83	5.10	1.24	2515	17	A	1.26	4.69	*
848	-	-	-	42097	122552.78	54829.5	Im pec/BCD	14.72	1.16	0.98	1537	23	B	6.70	2.86	
857	4394	-	7523	99047	122555.64	181249.5	SBb(sr)	11.76	3.60	3.60	914	17	A	5.94	5.64	*
873	4402	-	7528	70071	122607.32	130643.6	Sc (on edge)	12.56	3.95	1.16	234	17	A	1.36	2.95	
890	-	-	-	-	122620.85	64005.7	BCD	16.00	0.21	0.21	1483	23	B	5.83	2.64	
912	4413	-	7538	70076	122632.16	123639.8	SBbc(rs)	12.97	2.92	1.75	105	17	A	1.07	3.14	
945	-	3355	7548	70085	122651.06	131032.9	SBm	15.31	1.29	0.57	-9	17	A	1.25	2.67	
950	-	3356	7547	70084	122651.38	113316.9	Sm	14.49	1.71	0.85	1098	17	A	1.28	2.78	
971	4423	-	7556	42107	122708.93	55248.1	Sd (on edge)	14.28	3.06	0.43	1120	23	B	6.57	3.44	
984	4425	-	7562	70091	122713.30	124405.1	SBa	12.82	2.99	1.00	1883	17	A	0.94	4.68	
995	-	3371	7565	70092	122721.55	105155.2	Sc (on edge)	15.32	1.53	0.11	928	17	A	1.75	3.43	
1001	-	-	-	-	122724.65	134300.2	Im	16.60	0.73	0.47	338	17	A	1.56	2.44	
1002	4430	-	7566	42111	122726.37	61544.2	SBc(r)	12.48	3.02	2.69	1450	23	B	6.19	2.73	
1003	4429	-	7568	70093	122726.31	110629.2	S0/Sa pec	11.15	8.12	3.52	1130	17	A	1.53	5.48	*
1043	4438	-	7574	70097	122745.52	130031.4	Sb (tides)	10.91	8.12	3.68	70	17	A	0.97	10.21	*
1047	4440	-	7581	70099	122753.52	121735.5	SBa(sr)	12.48	2.01	1.71	724	17	A	0.72	7.42	
1106	-	-	-	-	122829.23	103112.8	Im:	17.50	0.59	0.41	-	17	A	1.96	2.26	
1110	4450	-	7594	99062	122829.27	170506.8	Sab pec	10.93	6.15	4.04	1954	17	A	4.73	4.33	*
1121	-	-	-	-	122841.73	110754.9	Im?	16.48	0.71	0.56	-	17	A	1.36	-	
1158	4461	-	7613	70115	122903.01	131101.1	Sa	12.09	3.52	1.29	1919	17	A	0.90	7.45	
1189	-	3414	7621	42129	122928.83	64612.3	Sc(s)	13.70	1.84	1.07	597	17	S	5.63	2.42	
1196	4468	-	7628	70122	122931.25	140258.3	S0/Sa	13.80	1.76	1.06	895	17	A	1.69	4.31	
1200	-	3416	-	70124	122934.53	104737.3	Im	15.10	1.26	0.84	-123	17	A	1.63	2.76	
1217	-	3418	7630	-	122942.54	112404.4	SBm	14.59	1.87	1.29	-	17	A	1.03	2.80	
1253	4477	-	7638	70129	123002.37	133810.6	SB0/SBa	11.31	3.60	3.60	1353	17	A	1.26	8.73	*
1257	-	-	-	-	123004.68	172401.6	Im pec	16.50	1.36	0.32	2488	17	A	5.01	2.55	
1287	-	-	-	-	123023.79	135855.8	Im	16.00	0.85	0.85	-	17	A	1.59	-	
1313	-	-	-	-	123048.47	120242.0	BCD	17.15	0.45	0.20	1254	17	A	0.35	2.07	
1326	4491	-	7657	70140	123057.15	112859.1	SBa(s)	13.41	1.89	0.94	497	17	A	0.91	2.87	
1356	-	3446	-	70142	123122.92	112934.3	Sm/BCD	15.55	1.10	0.43	1251	17	A	0.91	2.71	
1368	4497	-	7665	70145	123132.79	113736.4	SB0/SBa	13.12	2.01	0.85	1123	17	A	0.78	2.81	
1377	-	-	-	-	123139.21	105008.5	Im:	16.87	0.61	0.43	-	17	A	1.57	2.79	
1379	4498	-	7669	99075	123139.62	165107.5	SBc(s)	12.62	2.85	1.53	1505	17	A	4.46	2.27	
1403	-	-	-	-	123159.63	130459.7	Im?	17.15	0.71	0.43	-	17	A	0.75	-	
1410	4502	-	7677	99078	123203.22	164114.7	Sm	14.57	1.48	0.78	1629	17	A	4.31	2.80	
1411	-	3466	-	70150	123204.83	114902.7	pec,N	15.72	0.70	0.43	911	17	A	0.65	2.74	
1412	4503	-	7680	70149	123206.13	111034.8	Sa	12.12	4.33	1.71	1342	17	A	1.25	5.95	
1419	4506	-	7682	70152	123210.46	132509.8	Spec(dust)	13.64	2.16	1.29	737	17	A	1.08	3.44	
1426	-	-	-	-	123222.80	115338.9	Im?	15.64	0.80	0.80	1110	17	A	0.63	3.08	
1448	-	3475	7692	70156	123240.83	124613.1	Im	13.87	2.31	1.83	2583	17	A	0.59	2.88	
1450	-	3476	7695	70157	123241.91	140256.1	Sc(s)	13.29	2.60	2.01	-173	17	A	1.72	2.93	
1486	-	3483	-	70160	123309.94	112049.4	Spec,N	15.30	1.10	0.78	129	17	A	1.19	7.18	
1552	4531	-	7729	70175	123415.77	130429.1	Sa pec	12.58	4.24	2.42	195	17	A	1.08	3.00	
1554	4532	-	7726	42158	123419.31	62807.1	Sm	12.30	2.60	1.00	2021	17	S	5.99	2.92	
1569	-	3520	-	70178	123431.68	133013.2	Scd:	15.00	1.07	0.71	799	17	A	1.43	3.16	
1575	-	3521	7736	42162	123439.28	70938.3	SBm pec	13.98	2.00	1.41	597	17	S	5.32	2.44	
1581	-	-	7739	42163	123444.93	61807.4	Sm	14.55	1.46	1.16	2065	17	S	6.17	2.77	
1596	-	-	-	-	123500.91	91116.5	Im:	17.24	0.35	0.16	1286	17	S	3.36	-	

Table 2: continue

VCC	NGC	IC	UGC	CGCG	R.A.(2000)	dec	type	m_{pg}	a	b	vel	$Dist$	memb.	θ	C_{31}	com
					h m s	o ' "		mag	'	'	km s^{-1}	Mpc		deg		
(1)	(2)	(3)	(4)	(5)	(6)	(7)	(8)	(9)	(10)	(11)	(12)	(13)	(14)	(15)	(16)	(17)
1644	-	-	-	-	123551.82	135133.1	Sm	17.50	0.98	0.17	756	17	A	1.91	2.93	
1673	4567	-	7777	70189	123632.66	111528.6	Sc(s)	12.08	2.92	1.87	2277	17	A	1.80	2.73	*
1675	-	-	-	42174	123634.65	80317.6	Pec	14.47	1.26	0.74	1795	17	S	4.56	2.87	
1676	4568	-	7776	70188	123634.16	111419.6	Sc(s)	11.70	5.10	1.75	2255	17	A	1.82	4.27	*
1678	-	3576	7781	42176	123637.61	63716.6	SBd	13.70	2.16	1.87	1073	17	S	5.94	2.91	*
1686	-	3583	7784	70191	123643.57	131531.7	Sm	13.95	2.79	1.71	1122	17	A	1.68	2.98	
1690	4569	-	7786	70192	123649.78	130945.7	Sab(s)	10.25	10.73	5.35	-216	17	A	1.65	4.37	*
1699	-	3589	7790	42179	123702.24	65530.9	SBm	14.11	1.55	0.83	1635	17	S	5.68	2.64	
1725	-	-	-	70196	123741.51	83331.3	Sm/BCD	14.51	1.55	0.97	1068	17	S	4.19	2.92	
1726	-	-	7795	42184	123745.08	70622.4	Sdm	14.54	1.29	1.00	61	17	S	5.55	2.73	
1727	4579	-	7796	70197	123743.48	114904.4	Sab(s)	10.56	6.29	4.87	1520	17	A	1.78	4.51	*
1730	4580	-	7794	42183	123748.60	52206.4	Sc/Sa	12.61	2.16	1.60	1032	17	S	7.23	2.68	
1750	-	-	-	-	123815.48	65938.7	BCD?	16.50	0.31	0.16	-117	17	S	5.70	2.54	
1757	4584	-	7803	70199	123817.79	130635.8	Sa(s)pec	13.60	1.87	1.00	1783	17	A	1.96	3.53	
1758	-	-	7802	42186	123820.81	75328.8	Sc (on edge)	14.99	1.71	0.27	1788	17	S	4.87	3.47	
1784	-	-	-	-	123913.81	153749.4	Im	15.84	0.79	0.63	57	17	E	3.83	2.80	
1789	-	-	-	42192	123921.34	45619.5	Im	15.07	1.10	0.62	1619	17	S	7.74	2.46	
1791	-	3617	7822	42194	123924.55	75752.5	SBm/BCD	14.67	1.29	0.64	2079	17	S	4.90	2.86	
1804	-	-	-	-	123940.25	92355.7	Im/BCD	15.63	0.75	0.30	1898	17	E	3.70	4.33	
1811	4595	-	7826	99106	123951.63	151753.9	Sc(s)	12.92	2.16	1.42	632	17	E	3.64	2.71	
1813	4596	-	7828	70206	123955.88	101034.9	SBa	11.51	4.76	4.04	1834	17	E	3.14	5.44	
1822	-	-	-	-	124010.14	65050.1	Im	15.60	0.63	0.25	1012	17	S	6.00	2.79	
1869	4608	-	7842	70214	124113.52	100922.9	SB0/a	12.05	4.30	3.42	1864	17	E	3.39	9.68	
1885	-	-	-	-	124137.57	154933.2	Im	16.41	1.16	0.57	-	17	E	4.32	2.80	
1918	-	-	-	-	124218.10	54421.7	Im	15.80	1.03	0.36	980	17	S	7.23	2.81	
1929	4633	-	7874	99111	124237.12	142122.0	Scd(s)	13.77	2.48	1.07	291	17	E	3.48	3.14	
1932	4634	-	7875	99112	124240.83	141746.0	Sc (on edge)	13.19	2.92	0.87	116	17	E	3.45	3.08	
1952	-	-	-	-	124306.86	73858.4	Im	16.00	0.71	0.35	1308	17	E	5.62	2.93	
1970	-	-	-	71013	124329.11	100534.7	Im,N?	15.80	0.71	0.50	1325	17	E	3.86	2.94	
1972	4647	-	7896	71015	124332.28	113454.7	Sc(rs)	12.03	2.60	2.16	1422	17	E	3.21	3.06	*
1987	4654	-	7902	71019	124356.71	130734.0	SBc(rs)	11.14	4.99	2.60	1039	17	E	3.28	2.93	
1992	-	-	7906	-	124410.02	120659.2	Im	15.50	0.81	0.51	1003	17	E	3.27	2.80	
1999	4659	-	7915	71024	124429.38	132953.5	Sa	13.08	1.99	1.25	267	17	E	3.51	6.03	
2006	-	3718	7920	71026	124445.93	122111.7	Amorphous	13.68	2.60	0.71	844	17	E	3.40	3.19	
2007	-	3716	-	43016	124447.50	80629.7	Im/BCD:	15.20	0.78	0.41	1857	17	E	5.49	2.70	
2023	-	3742	7932	71032	124531.55	131951.3	SBc(s)	13.86	2.01	1.00	958	17	E	3.70	3.09	
2033	-	-	-	71033	124604.76	82830.8	BCD	14.65	0.73	0.73	1486	17	E	5.42	3.70	
2034	-	-	-	-	124607.96	100948.8	Im	15.82	0.78	0.52	1500	17	E	4.36	2.46	
2037	-	-	-	-	124615.15	101224.9	Im/BCD	15.92	0.88	0.38	1142	17	E	4.37	2.92	
2058	4689	-	7965	71043	124745.39	134548.3	Sc(s)	11.55	5.86	4.44	1620	17	E	4.34	2.80	
2066	4694	-	7969	71044	124815.05	105906.7	Amorphous	12.19	3.20	1.16	1181	17	E	4.49	4.21	*
2070	4698	-	7970	71045	124822.96	82913.8	Sa	11.53	5.67	2.84	1008	17	E	5.82	5.78	*
2087	4733	-	7997	71054	125106.81	105444.3	SB0/a	12.63	1.96	1.96	908	17	E	5.18	2.73	
2094	-	-	-	-	125235.75	102648.7	Im:	17.80	0.37	0.37	-	17	E	5.68	-	

Notes on morphological type, from NED:

VCC 66: HII; VCC 92: M98: HII and Seyfert; VCC 460: LINER; VCC 836: Seyfert2; VCC 857: LINER; VCC 1003: HII LINER; VCC 1043: LINER, tidally interacting with VCC 1030; VCC 1110: LINER; VCC 1253: Seyfert 2; VCC 1673: interacting with VCC 1676?; VCC 1676: interacting with VCC 1673?; VCC 1678: HII; VCC 1690: M90: LINER, Seyfert; VCC 1727: M58; LINER, Seyfert 1.9; VCC 1972: interacting with VCC 1978 (M60)?; VCC 2066: HII; VCC 2070: Seyfert 2;

Table 3: The photometric data

VCC	UV	U	B	V	J	H	K	C6.75	I12	C15	I25	I60	P60	I100	P100	P170	r2.8	r6.3	r12.6	r21
λ	2000Å	3650Å	4400Å	5500Å	1.25μm	1.65μm	2.1μm	6.75μm	12μm	15μm	25μm	60μm	60μm	100μm	100μm	170μm	2.8cm	6.3cm	12.6cm	21cm
units	mag	mag	mag	mag	mag	mag	mag	mJy	mJy	mJy	mJy	mJy	mJy	mJy	mJy	mJy	mJy	mJy	mJy	mJy
(1)	(2)	(3)	(4)	(5)	(6)	(7)	(8)	(9)	(10)	(11)	(12)	(13)	(14)	(15)	(16)	(17)	(18)	(19)	(20)	(21)
1	-	-	15.90	15.13	13.58	12.81	12.52	1.15	-	2.86	<340	<390	100	<840	140	330	-	-	-	<1800
4	-	-	-	-	-	-	15.32	<1.31	-	<1.94	<340	<390	-	<840	-	-	-	-	-	<1800
17	-	-	16.28	15.89	14.81	14.30	14.15	0.98	-	1.76	130	130	<40	460	<30	<70	-	-	-	<1800
24	-	-	15.79	15.19	-	-	12.82	0.37	<80	0.82	<110	<120	<40	<300	<40	120	-	-	-	<1800
26	-	-	-	-	-	-	15.96	<0.71	-	<1.05	<340	<390	-	<840	-	-	-	-	-	<1800
66	12.00	11.91	11.98	11.39	9.89	9.14	8.92	229.59	110	192.69	<140	2110	2470	8080	5090	11270	6000	29000	13000	26200
81	-	-	15.85	15.30	-	-	13.21	<5.86	-	<6.94	<340	<390	<40	<840	<30	770	-	-	-	<1800
87	-	15.10	15.27	14.80	-	-	13.08	2.18	-	0.74	<340	<390	100	<840	150	380	-	-	-	<1800
92	11.17	11.17	10.73	9.83	7.72	6.85	6.59	900.15	1100	692.42	1460	8110	4700	23070	11460	40290	18000	33000	37000	73300
130	-	-	-	-	-	-	14.71	<0.96	<120	<1.42	<170	<110	<50	<280	70	80	-	-	-	<1800
152	-	13.78	13.56	12.72	-	9.75	9.49	173.99	230	145.13	240	3080	1870	7470	5480	8380	-	-	11000	19800
159	-	-	16.02	15.66	-	-	14.09	<3.30	-	<4.88	<340	<390	<40	<840	<40	160	-	-	-	<1800
169	-	-	-	-	-	-	-	<2.23	-	<3.3	<340	<390	<30	<840	<50	<50	-	-	-	<1800
171	-	-	-	-	-	-	-	<1.25	-	<1.85	<340	<390	-	<840	-	-	-	-	-	<1800
207	-	-	-	-	-	-	14.88	<0.25	<120	<0.42	<160	<140	-	<340	-	-	-	-	-	<1800
318	13.47	14.26	14.45	14.09	-	-	11.95	3.08	-	5.16	<740	240	130	620	350	960	-	-	-	<1800
425	-	-	-	-	-	-	-	<1.00	-	<1.33	<340	<390	-	<840	-	-	-	-	-	<1800
459	13.49	-	-	-	-	-	12.60	2.87	<100	2.96	<130	240	130	540	380	500	-	-	-	<1800
460	-	12.01	11.45	10.50	8.39	7.49	7.33	195.11	180	186.36	510	4580	3290	10390	9110	11250	6000	11000	20000	19100
655	-	13.62	13.59	12.93	-	-	10.29	42.05	<140	15.17	140	470	420	1890	1110	5360	-	-	1000	<1800
664	13.15	13.25	13.60	13.16	-	-	11.29	7.09	<70	15.17	140	600	750	1030	770	970	-	-	-	<1800
666	-	-	-	-	-	-	14.46	<4.34	-	<6.17	<340	<390	<30	<840	<30	<40	-	-	-	<1800
692	13.05	13.07	12.99	12.52	-	10.34	10.19	33.64	<90	25.22	<180	710	540	2010	1430	3910	-	2000	<4000	<1800
793	-	17.27	17.26	16.89	15.55	14.97	15.16	<99	-	<99	<340	<390	-	<840	-	-	-	-	-	<1800
802	-	17.15	17.61	-	-	-	14.81	<99	<100	<99	<170	<130	-	<620	-	-	-	-	-	<1800
809	15.14	15.14	15.11	14.43	-	-	12.03	5.97	-	3.57	<500	<470	-	<1100	-	-	-	-	-	<1800
836	12.56	12.00	11.86	11.11	9.32	8.37	7.92	528.11	1060	1064.56	3420	10050	7030	17400	14220	11630	36000	84000	129000	119400
848	-	15.01	15.18	14.76	-	-	12.91	1.20	-	<10.25	<340	<390	<60	<840	50	1410	-	-	-	<1800
857	-	12.28	11.92	11.09	-	-	8.02	114.95	150	98.3	150	960	650	4020	2830	7760	-	2000	<4000	700
873	13.72	13.02	12.64	11.80	-	8.67	8.39	500.01	790	525.45	640	5430	3820	17480	8610	17720	12000	21000	50000	59500
890	-	-	-	-	-	-	14.61	<0.27	<90	<0.32	<190	<150	<40	<360	<30	120	-	-	-	<1800
912	13.40	13.01	12.97	12.34	-	9.73	9.53	60.94	140	54.72	180	1000	830	3100	2340	2820	-	<1000	6000	<1800
945	14.32	15.24	15.47	15.15	-	-	13.45	<99	-	<99	<340	<390	-	<840	-	-	-	-	-	<1800
950	14.94	15.60	15.76	15.32	-	-	13.85	<99	-	<99	<340	<390	-	<840	-	-	-	-	-	<1800
971	13.32	14.06	14.17	13.61	-	-	11.32	8.21	<90	6.57	<140	470	290	1100	830	1380	-	-	-	3600
984	16.29	13.27	12.86	11.95	10.08	9.36	8.95	19.56	<120	9.69	<170	<180	<40	<340	<40	<170	-	<1000	<4000	<1800
995	-	15.21	15.39	14.78	-	-	12.61	1.40	-	3.02	<340	<390	-	<840	-	-	-	-	-	<1800
1001	-	-	-	-	-	-	14.79	<99	-	<99	<340	<390	-	<840	<20	230	-	-	-	<1800
1002	12.66	-	12.74	12.09	10.54	9.63	9.33	119.35	130	72.17	230	1150	940	3780	3360	5300	-	2000	4000	7900
1003	14.98	11.51	10.95	9.96	7.69	6.90	6.63	267.86	310	192.87	220	1510	870	4130	3940	3120	-	1000	<4000	<1800
1043	12.58	11.64	11.08	10.07	8.13	7.35	6.89	259.53	210	247.26	170	3760	2360	11270	7670	16720	44000	97000	109000	148900
1047	16.27	-	12.85	11.88	10.02	9.05	8.92	<99	<150	5.09	<160	210	<40	<280	<40	<210	<1000	-	27000	<4000
1106	-	-	-	-	-	-	15.00	<99	-	<99	<340	<390	-	<840	-	-	-	-	-	<1800
1110	-	11.48	10.96	10.07	7.74	7.03	6.74	236.00	150	252.78	170	1800	1790	7910	4080	10010	14000	28000	11000	10200
1121	-	-	-	-	-	-	15.22	<99	-	<99	<340	<390	-	<840	<20	<140	-	-	-	<1800
1158	15.26	12.72	12.19	11.23	8.91	8.22	7.99	44.15	<120	16.45	<180	<120	<40	<310	<50	<140	-	<1000	<4000	<1800
1189	13.35	13.90	14.02	13.56	-	-	11.32	12.89	<60	5.8	<170	230	180	730	490	1160	-	-	-	<1800
1196	-	14.32	13.92	13.07	11.03	10.38	10.17	6.03	-	1.82	<100	<180	<40	<420	<40	1240	-	-	-	<1800
1200	-	15.33	15.56	15.06	-	13.35	13.01	<99	-	<99	<340	<390	-	<840	-	-	-	-	-	13000
1217	15.49	-	14.52	14.17	13.26	12.72	12.55	3.65	-	<21.75	<340	<390	<40	<840	<30	<70	-	-	-	<1800
1253	-	12.11	11.52	10.57	8.26	7.51	7.25	96.85	<100	28.74	<170	540	140	1180	810	1130	<500	5000	8000	<1800
1257	-	-	-	-	-	-	14.08	<2.65	-	1.75	<340	<390	-	<840	-	-	-	-	-	<1800
1287	-	-	-	-	-	-	-	<99	-	<99	<340	<390	-	<840	-	-	-	-	-	<1800
1313	15.35	16.67	17.30	16.96	-	15.58	-	<99	<150	<99	<110	<140	-	<350	-	-	-	-	-	<19800
1326	15.01	13.74	13.52	12.69	-	10.07	9.95	27.00	<90	70.1	420	2770	2360	3490	2890	2980	5000	-	<4000	<1800
1356	14.65	15.35	15.56	15.11	-	-	12.84	-	-	-	<340	<390	-	<840	-	-	-	-	-	<1800

Table 3: continue

VCC	UV	U	B	V	J	H	K	C6.75	I12	C15	I25	I60	P60	I100	P100	P170	r2.8	r6.3	r12.6	r21
λ	2000Å	3650Å	4400Å	5500Å	1.25μm	1.65μm	2.1μm	6.75μm	12μm	15μm	25μm	60μm	60μm	100μm	100μm	170μm	2.8cm	6.3cm	12.6cm	21cm
units	mag	mag	mag	mag	mag	mag	mag	mJy	mJy	mJy	mJy	mJy	mJy	mJy	mJy	mJy	mJy	mJy	mJy	mJy
(1)	(2)	(3)	(4)	(5)	(6)	(7)	(8)	(9)	(10)	(11)	(12)	(13)	(14)	(15)	(16)	(17)	(18)	(19)	(20)	(21)
1368	17.22	13.76	13.44	12.56	-	9.88	9.70	8.62	<120	3.59	<130	<240	<150	<890	<30	200	-	-	9000	<4000
1377	-	-	17.23	16.49	-	-	14.06	<99	-	<99	<340	<390	-	<840	-	-	-	-	-	<1800
1379	12.31	12.71	12.76	12.17	-	9.97	9.74	95.88	150	62.02	90	1200	1140	3700	3270	4980	1000	-	-	4600
1403	-	-	-	-	-	-	-	<99	-	<99	<340	<390	-	<840	-	-	-	-	-	<4000
1410	-	14.46	14.54	14.05	-	-	11.93	9.68	-	4.51	<190	230	220	620	360	690	-	-	-	<1800
1411	16.10	-	15.99	15.49	-	-	13.61	<99	-	<99	<340	<390	-	<840	-	-	-	-	-	<4000
1412	-	12.79	12.18	11.18	8.91	8.18	7.88	47.83	<150	13.47	<140	<150	<60	<390	<70	710	-	<1000	8000	<1800
1419	-	14.10	13.82	13.00	-	10.38	10.32	16.31	-	12.5	<240	150	60	640	280	440	-	-	-	<1800
1426	-	-	16.43	15.73	-	-	13.48	<99	-	<99	<340	<390	-	<840	-	-	-	-	-	<4000
1448	-	14.70	14.55	13.87	12.40	11.68	11.50	<99	<100	<99	<180	<200	-	<340	-	-	-	-	-	6300
1450	12.53	-	13.43	12.98	-	10.82	10.55	72.46	190	59.61	350	1850	740	3100	2990	3960	10000	24000	15000	10100
1486	-	15.02	14.99	14.31	-	-	11.54	<99	-	<99	<340	<390	-	<840	-	-	-	-	-	<1800
1552	-	12.85	12.52	11.65	9.66	8.91	8.75	40.15	<100	27.73	<140	360	290	1720	1080	1940	<1000	-	6000	<1800
1554	11.34	12.01	12.35	11.96	10.39	9.67	9.39	183.96	290	213.47	830	8930	5560	15530	9070	10650	19000	58000	84000	123800
1569	-	15.73	15.86	15.39	-	-	13.50	0.80	-	<5.48	<340	<390	<50	<840	<50	<60	-	-	-	<1800
1575	13.80	13.76	13.79	13.13	-	-	10.54	47.48	<90	46.02	<150	1030	1110	2300	2080	2740	-	-	-	4200
1581	-	15.08	15.08	14.51	-	-	12.59	<10.32	-	<12.22	<340	<390	<30	<840	<30	330	-	-	-	<1800
1596	-	-	-	-	-	-	-	<0.30	-	<0.5	<340	<390	-	<840	-	-	-	-	-	<1800
1644	-	-	-	-	-	-	15.19	<99	-	<99	<340	<390	-	<840	-	-	-	-	-	<1800
1673	12.29	-	11.17	10.49	9.32	8.60	7.93	324.33	-	319.63	<240	<390	-	<840	-	-	-	-	<54000	10500
1675	-	-	-	-	-	-	12.30	<4.97	-	<8.41	<340	<390	50	<840	<30	160	-	-	-	<1800
1676	-	-	11.17	10.25	-	-	7.34	973.91	2000	1050.86	2580	20360	-	56810	-	-	29000	65000	75000	124200
1678	13.26	14.32	14.47	13.96	-	-	12.02	<21.54	<100	<29.13	<120	300	80	520	430	680	-	-	-	<1800
1686	-	13.00	13.46	13.03	-	-	11.22	25.19	<120	19.42	<180	540	450	1720	1130	1490	-	-	-	<1800
1690	11.67	10.34	10.10	9.32	7.54	6.81	6.66	830.16	1310	972.71	2070	10080	6200	26600	16000	29160	30000	40000	63000	72500
1699	13.43	14.38	14.46	14.04	-	-	12.19	4.15	-	14.04	<340	<390	270	<840	390	490	-	-	-	<1800
1725	13.47	14.26	14.61	14.23	13.13	12.51	12.26	2.32	60	2.7	100	<180	50	350	300	480	-	-	-	<1800
1726	13.83	14.93	15.36	15.13	-	-	13.38	<5.90	-	<9.3	<340	<390	<50	<840	<50	240	-	-	-	<1800
1727	12.60	11.05	10.51	9.64	7.48	6.72	6.42	658.15	1110	646.18	760	5850	4160	20860	12340	29190	82000	99000	95000	97400
1730	-	13.01	12.78	11.94	9.86	8.84	8.79	99.75	260	97.4	540	1460	1520	4820	3640	5460	<400	3000	<4000	<1800
1750	-	-	-	-	-	-	14.43	0.28	<130	<0.54	<170	<140	<30	<210	40	80	-	-	-	<1800
1757	-	14.08	13.90	13.14	-	-	10.52	<9.97	<100	<16.86	<140	240	100	<640	500	790	-	-	-	<1800
1758	-	14.98	15.00	14.37	-	-	11.85	5.92	-	0.98	<340	<390	-	<840	-	-	-	-	-	<1800
1784	-	-	-	-	-	-	14.74	<3.03	-	<6.28	<340	<390	-	<840	-	-	-	-	-	3500
1789	-	16.00	15.91	15.19	13.23	12.60	12.71	2.40	-	<7.38	<340	<390	-	<840	-	-	-	-	-	<1800
1791	13.07	14.41	14.67	14.37	-	-	12.49	2.88	-	3.97	<230	270	-	630	-	-	-	-	-	3000
1804	-	16.33	16.30	15.73	-	-	13.44	0.41	-	<2.43	<340	<390	-	<840	-	-	-	-	-	<1800
1811	12.81	13.11	13.11	12.56	-	10.22	10.04	74.49	100	52.59	180	900	-	2670	-	-	1000	7000	5000	7100
1813	13.78	12.01	11.48	10.53	8.17	7.44	7.19	126.86	120	40.01	<130	490	-	1280	-	-	-	<1000	4000	<1800
1822	-	16.63	16.85	16.49	-	-	14.36	0.72	-	<1.14	<340	<390	-	<840	-	-	-	-	-	<1800
1869	-	-	12.11	11.16	8.77	8.09	7.86	<99	<120	<99	<180	<150	-	<340	-	-	-	<1000	2000	2800
1885	-	-	-	-	-	-	14.06	<3.53	-	<5.96	<340	<390	-	<840	-	-	-	-	-	<1800
1918	-	-	-	-	-	-	14.47	0.87	-	1	<340	<390	-	<840	-	-	-	-	-	<1800
1929	12.87	13.63	13.77	13.19	-	-	10.61	29.28	<100	35.14	<130	500	-	1810	-	-	-	-	-	<1800
1932	-	13.25	13.18	12.45	10.52	9.67	9.25	290.08	400	265.79	480	4130	-	12650	-	-	6000	20000	20000	34000
1952	-	-	-	-	-	-	14.68	<1.51	-	<1.79	<240	<150	-	250	-	-	-	-	-	<1800
1970	-	-	-	-	-	-	13.75	<2.16	-	<3.2	<340	<390	-	<840	-	-	-	-	-	<1800
1972	11.88	12.36	12.02	11.34	10.14	8.74	8.58	501.09	980	493.38	780	5350	-	16040	-	-	6000	38000	26000	56300
1987	11.23	11.37	11.31	10.60	8.71	7.86	7.57	1051.86	1190	1101.42	1910	13930	-	37160	-	-	29000	51000	59000	125300
1992	-	16.08	16.58	16.15	15.48	14.88	14.54	0.58	-	<3.72	<340	<390	-	<840	-	-	-	-	-	<1800
1999	-	13.57	13.20	12.34	10.43	9.62	9.35	10.06	120	3.98	<80	<140	-	<570	-	-	-	-	<4000	<1800
2006	-	-	-	-	-	-	11.15	2.93	<120	1.49	<140	<150	-	<340	-	-	-	-	-	<1800
2007	-	-	-	-	-	-	13.35	1.80	-	<3.46	<340	<390	-	<840	-	-	-	-	-	<1800
2023	-	14.02	14.05	13.56	-	-	11.41	5.46	-	5.45	<100	250	-	940	-	-	-	-	-	<1800
2033	-	15.37	15.60	15.08	-	-	13.03	0.59	<110	1.17	<170	200	-	<350	-	-	-	-	-	<1800

Table 3: continue

VCC	UV	U	B	V	J	H	K	C6.75	I12	C15	I25	I60	P60	I100	P100	P170	r2.8	r6.3	r12.6	r21
λ	2000Å	3650Å	4400Å	5500Å	1.25μm	1.65μm	2.1μm	6.75μm	12μm	15μm	25μm	60μm	60μm	100μm	100μm	170μm	2.8cm	6.3cm	12.6cm	21cm
units	mag	mag	mag	mag	mag	mag	mag	mJy	mJy	mJy	mJy	mJy	mJy	mJy	mJy	mJy	mJy	mJy	mJy	mJy
(1)	(2)	(3)	(4)	(5)	(6)	(7)	(8)	(9)	(10)	(11)	(12)	(13)	(14)	(15)	(16)	(17)	(18)	(19)	(20)	(21)
2034	-	-	16.24	15.78	-	-	13.37	0.19	-	<3.66	<340	<390	-	<840	-	-	-	-	-	<1800
2037	-	16.12	16.20	15.79	-	-	13.49	<1.78	-	<2.11	<340	<390	-	<840	-	-	-	-	-	<1800
2058	12.62	-	11.73	10.98	-	8.43	7.88	316.50	380	352.68	400	3250	-	10490	-	-	3000	8000	7000	14300
2066	-	12.53	12.31	11.63	9.86	9.16	8.91	68.00	130	68.13	170	1170	-	2680	-	-	4000	3000	4000	4100
2070	-	11.99	11.48	10.56	8.25	7.57	7.31	88.49	280	66.58	<460	630	-	1890	-	-	-	2000	2000	<1800
2087	-	13.34	12.98	12.11	9.99	9.24	9.03	11.46	<120	7.06	<180	<130	-	<280	-	-	1000	-	<4000	<1800
2094	-	-	-	-	-	-	16.44	0.44	-	<1.23	<340	<390	-	<840	-	-	-	-	-	<1800

Note to Table 3:

VCC 1379: the 116000 mJy flux at 12.6 cm of Dressel & Condon is contaminated by a background quasar, visible in the NVSS 20cm map.

Table 4: References for the photometric data

VCC (1)	UV (2)	optical (3)	near-IR (4)	ISOCAM (5)	IRAS (6)	ISOPHOT (7)	radio 2.8cm (8)	radio 6.3cm (9)	radio 12.6cm (10)	radio 21cm (11)
1	-	1	1	1	1	1	-	-	-	1
4	-	-	3	1	1	-	-	-	-	1
17	-	2	1	1	9	1	-	-	-	1
24	-	1	1	1	2	1	-	-	-	1
26	-	-	3	1	1	-	-	-	-	1
66	1	1	1	1	4	1	1	1	-	1
81	-	1,2	1	1	1	1	-	-	-	1
87	-	3,4	1	1	1	1	-	-	-	1
92	1	1	1	1	3	1	1	1	1	3
130	-	-	3	1	2	1	-	-	-	1
152	-	1	1	1	6	1	-	-	-	1
159	-	2	1	1	1	1	-	-	-	1
169	-	-	-	1	1	1	-	-	-	1
171	-	-	-	1	1	-	-	-	-	1
207	-	-	3	1	2	-	-	-	-	1
318	1	3	1	1	10	1	-	-	-	1
425	-	-	-	1	1	-	-	-	-	1
459	1	-	1	1	2,7	1	-	-	-	1
460	-	1	1	1	4	1	1	1	1	1
655	-	4	1	1	4	1	-	-	-	1
664	1	7	1	1	2,4	1	-	-	-	1
666	-	-	3	1	1	1	-	-	-	1
692	3	5	1	1	4	1	-	1	-	1
793	-	1	3	1	1	-	-	-	-	1
802	-	4	3	-	2	-	-	-	-	1
809	3	3	1	1	10	-	-	-	-	1
836	3	1	1	1	3	1	1	1	1	1
848	-	4	1	1	1	1	-	-	-	1
857	-	1	1	1	4	1	-	1	-	4
873	3	1	1	1	3	1	1	1	1	2
890	-	-	1	1	2	1	-	-	-	1
912	3	3,7	1	1	2	1	-	1	-	1
945	3	4,6	1	-	1	-	-	-	-	1
950	3	3,4	1	-	1	-	-	-	-	1
971	1	3	1	1	4	1	-	-	-	1
984	3	1	1	1	2	1	-	1	-	1
995	-	2	1	1	1	-	-	-	-	1
1001	-	-	3	-	1	1	-	-	-	1
1002	1	1	1	1	2	1	-	1	-	1
1003	3	1	1	1	6	1	-	1	-	1
1043	3	1	1	1	4	1	1	1	1	2
1047	3	7	1,2	1	5	1	1	-	-	1
1106	-	-	3	-	1	-	-	-	-	1
1110	-	1	1	1	2	1	1	1	-	1
1121	-	-	3	-	1	1	-	-	-	1
1158	2	1	1	1	2	1	-	1	-	1
1189	1	3	1	1	4	1	-	-	-	1
1196	-	3,7,8	1	1	5	1	-	-	-	1
1200	-	4	1	-	1	-	-	-	-	1
1217	3	9	1	1	1	1	-	-	-	1
1253	-	1	1	1	4	1	1	1	-	1
1257	-	-	3	1	1	-	-	-	-	1
1287	-	-	-	-	1	-	-	-	-	1
1313	3	4	4	-	2	-	-	-	-	1
1326	3	3,7	1	1	4	1	1	-	-	1
1356	3	3	1	-	1	-	-	-	-	1
1368	3	3,7	1	1	5	1	-	-	-	1
1377	-	2	1	-	1	-	-	-	-	1
1379	1	5	1	1	2	1	1	-	-	1
1403	-	-	-	-	1	-	-	-	-	1
1410	-	1	1	1	7	1	-	-	-	1
1411	3	2	1	-	1	-	-	-	-	1
1412	-	1	1	1	2,8	1	1	-	-	1
1419	-	3	1	1	8	1	-	-	-	1
1426	-	2	1	-	1	-	-	-	-	1
1448	-	4,7	1	-	2	-	-	-	-	1
1450	1	7	1	1	2	1	1	1	-	1
1486	-	3,4	1	-	1	-	-	-	-	1
1552	-	1	1	1	2,4	1	1	-	-	1
1554	1	1	1	1	3	1	1	1	1	1
1569	-	3	1	1	1	1	-	-	-	1
1575	1	1	1	1	4	1	-	-	-	1
1581	-	4,7	1	1	1	1	-	-	-	1
1596	-	-	-	1	1	-	-	-	-	1

Table 4: continue

VCC (1)	UV (2)	optical (3)	near-IR (4)	ISOCAM (5)	IRAS (6)	ISOPHOT (7)	radio 2.8cm (8)	radio 6.3cm (9)	radio 12.6cm (10)	radio 21cm (11)
1644	-	-	3	-	1	-	-	-	-	1
1673	1	1	1	1	1	1	-	-	-	1
1675	-	-	1	1	1	1	-	-	-	1
1676	-	1	1	1	3	1	1	1	1	1
1678	1	7	1	1	2	1	-	-	-	1
1686	-	1	-	1	2	1	-	-	-	1
1690	1	1	1	1	3	1	1	1	1	1
1699	1	3	1	1	1	1	-	-	-	1
1725	1	3,4,10	1	1	9	1	-	-	-	1
1726	1	4	1	1	1	1	-	-	-	1
1727	1	1	1	1	3	1	1	1	1	1
1730	-	3,7	1	1	6	1	1	1	-	1
1750	-	-	3	1	2	1	-	-	-	1
1757	-	3,7	1	1	4,6	1	-	-	-	1
1758	-	3	1	1	1	-	-	-	-	1
1784	-	-	3	1	1	-	-	-	-	1
1789	-	4	1	1	1	-	-	-	-	1
1791	1	3,4,6	1	1	7	-	-	-	-	1
1804	-	2	1	1	1	-	-	-	-	1
1811	1	3,11	1	1	2	-	1	1	-	1
1813	1	1	1	1	7	-	-	1	-	1
1822	-	2	1	1	1	-	-	-	-	1
1869	-	1	1	-	2	-	-	1	-	1
1885	-	-	1	1	1	-	-	-	-	1
1918	-	-	1	1	1	-	-	-	-	1
1929	1	1	1	1	2	-	-	-	-	1
1932	-	1	1	1	6	-	1	1	1	1
1952	-	-	1	1	9	-	-	-	-	1
1970	-	-	1	1	1	-	-	-	-	1
1972	1	7	1	1	3	-	1	1	1	1
1987	1	1	1	1	3	-	1	1	1	1
1992	-	2	1	1	1	-	-	-	-	1
1999	-	3,11	1	1	4	-	-	-	-	1
2006	-	-	1	1	2	-	-	-	-	1
2007	-	-	1	1	1	-	-	-	-	1
2023	-	3	1	1	7	-	-	-	-	1
2033	-	4	1	1	2	-	-	-	-	1
2034	-	2	1	1	1	-	-	-	-	1
2037	-	2	1	1	1	-	-	-	-	1
2058	1	1	1	1	6	-	1	1	-	1
2066	-	1	1	1	4	-	1	1	-	1
2070	-	1	1	1	2	-	-	1	-	1
2087	-	12,13	1	1	2,5	-	1	-	-	1
2094	-	-	3	1	1	-	-	-	-	1

References:

UV data:

1: Deharveng et al. (1994) 2: Deharveng et al. (2002) 3: Donas et al. (private communication)

Optical data:

1: this work 2: Gavazzi et al. (2001) 3: Schroeder & Visvanathan (1996) 4: Gallagher & Hunter (1986) 5: Gavazzi et al. (1994) 6: de Vaucouleurs et al. (1981) 7: Longo et al. (1983-1985) 8: Prugniel & Heraudeau P. (1998) 9: Bothun et al. (1986) 10: Takamiya et al. (1995) 11: Boselli & Gavazzi (1994) 12: Burstein et al. (1987) 13: Frueh et al. (1996)

Near-IR:

1: Boselli et al. (1997) 2: Gavazzi et al. (2001) 3: Pierini, private communication 4: Gavazzi et al., in preparation

ISOCAM data:

1: Boselli et al. (2002c)

IRAS data:

1: Lonsdale et al. (1985) 2: Helou et al. (1988) 3: Soifer et al. (1989) 4: Thuan & Sauvage (1992) 5: Isobe & Feigelson (1992) 6: Rush et al. (1993) 7: Young et al. (1996) 8: Tuffs, private communication 9: Almoznino & Brosch (1998) 10: Magri (1994)

ISOPHOT data:

Tuffs et al. (2002)

Radio continuum data:

2.8cm:

1: Niklas et al. (1995)

6.3cm:

1: Niklas et al. (1995)

12.6cm:

1: Dressel & Condon (1978)

21cm:
1: Gavazzi & Boselli (1999) 2: Kotanyi et al. (1980) 3: Condon et al. (1990) 4: Condon et al. (1987)

Table 5: The emission lines data

VCC	$H\alpha+[NII]EW$ Å	$F(H\alpha+[NII])$ erg cm^{-2} s^{-1}	ref	MHI M⊙	$defHI$	qual	WHI km s^{-1}	ref	MH_2 M⊙	ref
(1)	(2)	(3)	(4)	(5)	(6)	(7)	(8)	(9)	(10)	(11)
1	12	-13.51	1	-	-	-	-	-	-	-
4	-	-	-	8.25	0.00	2	41	1	-	-
17	53	-12.83	6	8.78	-0.04	2	58	1	-	-
24	3	-14.03	1	8.93	-0.11	1	218	1	-	-
26	-	-	-	8.38	-0.26	3	47	1	-	-
66	33	-11.72	6	9.81	-0.20	1	269	9	7.75	3
81	21	-13.26	1	8.63	-0.45	1	103	3	-	-
87	20	-12.94	6	8.32	0.29	2	109	1	<8.13	4
92	9	-11.53	1	9.76	0.33	1	469	11	8.75	1
130	-	-	-	7.86	0.06	1	119	1	-	-
152	9	-12.63	6	8.61	0.24	1	216	5	8.15	3
159	19	-13.21	6	8.55	0.30	2	67	1	-	-
169	7	-14.36	4	8.52	-0.35	2	35	1	-	-
171	-	-	-	7.16	1.20	4	29	2	-	-
207	-	-	-	8.25	-0.25	2	81	2	-	-
318	51	-12.51	1	9.39	-0.13	1	178	5	<8.34	4
425	-	-	-	<7.53	0.33	-	-	2	-	-
459	48	-12.66	2	8.22	-0.07	2	127	1	<7.72	4
460	8	-11.92	6	7.62	1.85	3	274	6	8.43	1
655	6	-12.78	6	7.91	0.75	2	71	8	7.99	3
664	101	-12.12	1	8.40	0.62	2	103	7	<7.79	3
666	-	-	-	<7.60	0.71	-	-	1	-	-
692	16	-12.47	5	8.46	0.66	1	119	7	<7.60	3
793	2	-14.41	2	7.65	0.05	2	41	1	-	-
802	37	-13.54	2	<7.66	0.28	-	-	1	-	-
809	-	-	-	8.39	0.15	2	173	3	-	-
836	15	-11.67	1	8.78	0.69	1	394	7	8.29	3
848	26	-13.05	2	8.85	-0.18	2	141	1	-	-
857	12	-11.97	1	8.51	0.86	1	174	7	8.30	1
873	16	-11.97	2	8.74	0.63	1	269	4	8.96	1
890	-	-	-	7.33	-0.05	2	66	2	-	-
912	13	-12.56	6	8.26	0.99	1	157	7	8.12	3
945	-	-	-	8.21	0.31	3	37	1	-	-
950	23	-13.45	3	8.81	-0.07	2	74	1	-	-
971	29	-12.52	3	9.26	0.20	2	171	2	8.86	3
984	1	-13.17	1	<7.31	1.78	-	-	8	-	-
995	32	-12.98	6	8.92	-0.33	1	162	3	-	-
1001	-1	-	6	7.49	0.57	3	37	1	-	-
1002	9	-12.11	6	8.92	0.47	1	152	4	8.24	3
1003	5	-11.72	1	<7.44	2.30	-	-	8	7.39	7
1043	7	-11.77	6	8.62	1.33	2	253	8	8.98	5
1047	-1	-	6	<7.44	1.37	-	-	8	8.25	2
1106	-	-	-	<7.19	0.68	-	-	1	-	-
1110	2	-12.30	5	8.65	0.95	1	319	4	8.32	1
1121	-	-	-	<7.63	0.39	-	-	1	-	-
1158	-1	-	6	<7.13	2.07	-	-	6	-	-
1189	21	-12.67	6	8.39	0.34	3	126	5	<7.86	3
1196	-	-	-	-	-	-	-	-	-	-
1200	-	-13.61	-	<7.39	1.11	-	-	1	-	-
1217	-	-	-	<7.09	1.73	-	-	2	-	-
1253	-	-	-	<7.31	1.79	-	-	8	-	-
1257	-	-	-	8.41	0.14	1	157	1	-	-
1287	-	-	-	<7.63	0.54	-	-	1	-	-
1313	351	-12.84	2	7.84	-0.20	2	107	1	-	-
1326	-1	-	6	<7.24	1.52	-	-	6	7.98	3
1356	43	-13.05	1	8.34	0.04	1	168	3	-	-
1368	-	-	-	<7.38	1.28	-	-	8	-	-
1377	-	-	-	<7.53	0.37	-	-	1	-	-
1379	36	-11.92	3	8.95	0.15	1	200	4	7.84	3
1403	-	-	-	<7.57	0.45	-	-	1	-	-
1410	35	-12.71	1	8.20	0.42	1	181	1	-	-
1411	2	-14.37	3	7.96	0.51	3	57	1	-	-
1412	2	-12.52	1	<7.02	2.33	-	-	6	<7.76	4
1419	5	-13.06	6	<7.27	1.59	-	-	3	-	-
1426	6	-13.93	3	<7.33	0.79	-	-	1	-	-
1448	-	-	-	8.90	-0.14	5	70	13	-	-
1450	69	-11.89	1	8.47	0.54	1	130	10	7.78	3
1486	12	-13.17	6	7.66	0.72	2	124	5	-	-
1552	2	-12.98	1	<7.16	2.18	-	-	6	7.62	3
1554	75	-11.40	6	9.46	-0.37	1	185	4	8.02	4
1569	14	-13.45	6	7.47	0.90	2	109	3	-	-
1575	13	-12.73	1	7.94	0.93	2	113	5	8.62	3
1581	6	-13.46	3	8.64	-0.03	2	97	1	-	-
1596	-	-	-	7.34	0.12	4	56	1	-	-

Table 5: continue

VCC	$H\alpha+[NII]EW$	$F(H\alpha+[NII])$	ref	MHI	$defHI$	qual	WHI	ref	MH_2	ref
	Å	erg cm^{-2} s^{-1}		M⊙			km s^{-1}		M⊙	
(1)	(2)	(3)	(4)	(5)	(6)	(7)	(8)	(9)	(10)	(11)
1644	-	-	-	8.15	0.14	1	93	1	-	-
1673	15	-12.00	1	8.69	0.43	3	214	12	8.70	1
1675	4	-13.85	1	7.45	1.35	3	41	1	-	-
1676	19	-11.74	1	8.99	0.58	3	341	12	8.99	1
1678	55	-12.56	6	9.00	-0.06	2	57	5	-	-
1686	44	-12.17	1	8.35	0.79	1	116	1	<7.77	4
1690	2	-12.02	1	8.93	1.07	1	370	11	9.01	1
1699	24	-12.85	3	8.62	0.04	2	109	1	-	-
1725	50	-12.62	2	8.11	0.55	2	93	1	-	-
1726	-	-12.80	-	8.52	0.00	2	85	1	-	-
1727	4	-11.49	6	8.79	0.83	1	374	7	9.08	6
1730	4	-12.62	1	7.83	1.03	3	190	4	8.04	3
1750	-	-	-	7.35	-0.01	4	73	1	-	-
1757	7	-12.98	3	7.38	1.38	5	-	3	-	-
1758	17	-13.07	1	8.28	0.39	1	172	5	-	-
1784	2	-	4	7.34	0.78	4	37	1	-	-
1789	16	-13.25	3	7.86	0.53	1	103	1	-	-
1791	72	-12.42	3	8.63	-0.12	2	120	1	-	-
1804	3	-14.37	2	7.23	0.84	5	88	1	-	-
1811	16	-12.50	6	8.63	0.23	1	150	4	8.20	3
1813	-1	-	6	<7.19	2.23	-	-	6	<7.39	3
1822	-1	-	4	7.64	0.29	2	34	1	-	-
1869	-	-	-	<7.44	1.81	-	-	8	-	-
1885	-	-	-	<7.33	1.09	-	-	1	-	-
1918	15	-13.90	3	8.16	0.17	2	77	1	-	-
1929	13	-12.75	6	8.70	0.35	1	190	10	<7.68	4
1932	16	-12.32	6	8.66	0.45	1	301	6	8.46	3
1952	32	-13.62	4	8.21	-0.19	2	65	1	-	-
1970	-	-	-	<7.49	0.53	-	-	1	-	-
1972	16	-11.71	6	8.75	0.27	1	203	4	8.69	1
1987	31	-11.34	6	9.85	-0.29	1	308	7	8.66	1
1992	24	-13.21	4	8.35	-0.22	1	110	1	-	-
1999	-1	-	6	<7.19	1.61	-	-	6	-	-
2006	-1	-	6	7.94	0.91	2	78	3	-	-
2007	10	-13.77	2	7.37	0.74	3	77	1	-	-
2023	27	-12.56	3	8.85	-0.05	1	186	3	<7.93	4
2033	13	-13.32	2	7.45	0.61	3	41	1	-	-
2034	3	-14.28	6	7.83	0.27	3	62	1	-	-
2037	16	-13.82	6	7.39	0.81	3	44	1	-	-
2058	14	-11.85	6	8.79	0.90	1	195	4	8.70	1
2066	6	-12.47	6	8.36	0.66	2	106	1	7.71	3
2070	2	-11.98	6	9.54	0.01	1	432	4	<7.45	5
2087	-	-	-	<7.38	1.26	-	-	8	-	-
2094	-	-	-	<7.09	0.40	-	-	2	-	-

References:

Hα+[NII]:

1: Boselli & Gavazzi (2002); 2: Boselli et al. (2002a); 3: Gavazzi et al. (2002b); 4: Heller et al. (1999); 5: Koopmann et al. (2001) (equivalent width from ref. 6);6: Boselli et al., in preparation

HI:

1: Hoffman et al. (1987); 2: Hoffman et al. (1989a); 3: Haynes & Giovanelli (1986); 4: Helou et al. (1984); 5: Hoffman et al. (1989b); 6: Magri (1994); 7: Helou et al. (1981); 8: Giovanardi et al. (1983); 9: Warmels (1986); 10: Schneider et al. (1990); 11: Huchtmeier et al. (1989); 12: Helou et al. (1982); 13: Bottinelli et al. (1990);

CO:

1: Kenney & Young (1988); 2: Stark et al. (1986); 3: Boselli et al. (1995); 4: Boselli et al. (2002b); 5: Combes et al. (1988); 6: Boselli et al., in preparation; 7: Sage & Wrobel (1989);

Table 7: The galactic and internal extinction corrections

VCC (1)	AB (2)	A(UV) (3)	A(U) (4)	A(B) (5)	A(V) (6)	A(J) (7)	A(H) (8)	A(K) (9)
1	0.02	-	-	0.35	0.25	0.07	0.05	0.03
4	0.12	-	-	-	-	-	-	0.03
17	0.08	-	-	0.41	0.31	0.07	0.05	0.03
24	0.01	-	-	0.34	0.25	-	-	0.03
26	0.13	-	-	-	-	-	-	0.03
66	0.00	0.68	0.39	0.33	0.25	0.07	0.05	0.04
81	0.14	-	-	0.58	0.43	-	-	0.05
87	0.08	-	0.47	0.41	0.31	-	-	0.03
92	0.14	1.20	0.70	0.60	0.46	0.11	0.07	0.05
130	0.00	-	-	-	-	-	-	0.03
152	0.00	-	0.50	0.43	0.33	-	0.07	0.05
159	0.00	-	-	0.33	0.24	-	-	0.03
169	0.00	-	-	-	-	-	-	-
171	0.00	-	-	-	-	-	-	-
207	0.00	-	-	-	-	-	-	0.03
318	0.00	0.24	0.14	0.11	0.07	-	-	0.01
425	0.00	-	-	-	-	-	-	-
459	0.04	0.31	-	-	-	-	-	0.01
460	0.07	-	0.88	0.77	0.59	0.16	0.11	0.08
655	0.03	-	0.42	0.36	0.27	-	-	0.03
664	0.07	0.56	0.29	0.25	0.19	-	-	0.02
666	0.03	-	-	-	-	-	-	0.03
692	0.01	0.56	0.33	0.28	0.20	-	0.04	0.03
793	0.12	-	0.53	0.45	0.33	0.07	0.05	0.03
802	0.11	-	0.51	0.44	-	-	-	0.03
809	0.05	0.95	0.55	0.48	0.37	-	-	0.05
836	0.11	2.00	1.28	1.13	0.88	0.25	0.17	0.12
848	0.00	-	0.39	0.33	0.24	-	-	0.03
857	0.03	-	0.83	0.72	0.56	-	-	0.08
873	0.12	2.66	1.73	1.54	1.25	-	0.29	0.21
890	0.00	-	-	-	-	-	-	0.03
912	0.10	1.12	0.66	0.57	0.43	-	0.07	0.05
945	0.12	0.93	0.52	0.45	0.34	-	-	0.03
950	0.03	0.74	0.42	0.36	0.27	-	-	0.03
971	0.00	0.43	0.23	0.2	0.14	-	-	0.02
984	0.10	1.49	0.92	0.81	0.62	0.16	0.11	0.08
995	0.10	-	0.62	0.53	0.40	-	-	0.05
1001	0.08	-	-	-	-	-	-	0.03
1002	0.00	0.64	-	0.32	0.23	0.07	0.05	0.03
1003	0.05	0.10	0.07	0.07	0.04	-	-	-
1043	0.09	1.45	0.88	0.76	0.59	0.16	0.11	0.08
1047	0.08	1.45	-	0.77	0.60	0.16	0.11	0.08
1106	0.01	-	-	-	-	-	-	0.03
1110	0.03	-	0.84	0.73	0.56	0.16	0.11	0.08
1121	0.04	-	-	-	-	-	-	0.03
1158	0.07	1.43	0.89	0.78	0.59	0.16	0.11	0.08
1189	0.00	0.23	0.12	0.10	0.07	-	-	0.01
1196	0.08	-	0.10	0.09	0.06	-	-	-
1200	0.03	-	0.42	0.36	0.28	-	0.05	0.03
1217	0.03	0.74	-	0.36	0.28	0.07	0.05	0.03
1253	0.02	-	0.04	0.04	0.02	-	-	-
1257	0.02	-	-	-	-	-	-	0.03
1287	0.08	-	-	-	-	-	-	-
1313	0.09	0.87	0.49	0.42	0.31	-	0.05	-
1326	0.02	2.54	1.69	1.51	1.24	-	0.31	0.22
1356	0.02	0.72	0.41	0.35	0.26	-	-	0.03
1368	0.04	0.08	0.06	0.06	0.04	-	-	-
1377	0.02	-	-	0.35	0.27	-	-	0.03
1379	0.03	0.55	0.31	0.26	0.19	-	0.03	0.02
1403	0.07	-	-	-	-	-	-	-
1410	0.03	-	0.43	0.36	0.27	-	-	0.03
1411	0.05	0.78	-	0.38	0.28	-	-	0.03
1412	0.01	-	0.81	0.71	0.55	0.16	0.11	0.08
1419	0.01	-	0.81	0.70	0.54	-	0.11	0.08
1426	0.08	-	-	0.41	0.31	-	-	0.03
1448	0.08	-	0.12	0.12	0.07	-	-	-
1450	0.11	0.89	-	0.43	0.33	-	0.05	0.03
1486	0.01	-	0.80	0.70	0.54	-	-	0.08
1552	0.08	-	0.88	0.77	0.60	0.16	0.11	0.08
1554	0.00	0.92	0.56	0.47	0.35	0.11	0.07	0.05
1569	0.08	-	0.60	0.51	0.39	-	-	0.05
1575	0.00	1.05	0.64	0.55	0.42	-	-	0.06
1581	0.00	-	0.40	0.33	0.24	-	-	0.03
1596	0.00	-	-	-	-	-	-	-

Table 7: continue

VCC (1)	AB (2)	A(UV) (3)	A(U) (4)	A(B) (5)	A(V) (6)	A(J) (7)	A(H) (8)	A(K) (9)
1644	0.10	-	-	-	-	-	-	0.03
1673	0.01	0.87	-	0.45	0.33	0.10	0.07	0.05
1675	0.00	-	-	-	-	-	-	0.03
1676	0.01	-	-	0.45	0.33	-	-	0.05
1678	0.00	0.19	0.10	0.08	0.06	-	-	0.01
1686	0.09	-	0.49	0.42	0.31	-	-	0.03
1690	0.09	1.50	0.91	0.79	0.62	0.17	0.11	0.08
1699	0.00	0.68	0.39	0.33	0.24	-	-	0.03
1725	0.00	0.68	0.39	0.33	0.25	0.07	0.05	0.03
1726	0.00	0.68	0.38	0.33	0.25	-	-	0.03
1727	0.14	1.95	1.23	1.07	0.84	0.23	0.16	0.11
1730	0.00	-	0.51	0.43	0.33	0.10	0.07	0.05
1750	0.00	-	-	-	-	-	-	0.03
1757	0.09	-	0.91	0.80	0.61	-	-	0.08
1758	0.00	-	0.51	0.44	0.33	-	-	0.05
1784	0.02	-	-	-	-	-	-	0.03
1789	0.00	-	0.39	0.33	0.24	0.07	0.05	0.03
1791	0.00	0.15	0.08	0.06	0.03	-	-	0.01
1804	0.00	-	0.39	0.33	0.24	-	-	0.03
1811	0.03	0.62	0.35	0.30	0.22	-	0.04	0.03
1813	0.00	0.67	0.39	0.35	0.25	0.07	0.05	0.03
1822	0.00	-	0.39	0.33	0.25	-	-	0.03
1869	0.00	-	-	0.03	0.01	-	-	-
1885	0.04	-	-	-	-	-	-	0.03
1918	0.02	-	-	-	-	-	-	0.03
1929	0.03	0.44	0.23	0.2	0.15	-	-	0.02
1932	0.03	-	0.53	0.46	0.35	0.10	0.07	0.05
1952	0.00	-	-	-	-	-	-	0.03
1970	0.00	-	-	-	-	-	-	0.03
1972	0.04	1.15	0.70	0.61	0.46	0.13	0.09	0.06
1987	0.06	1.39	0.85	0.74	0.57	0.16	0.11	0.08
1992	0.00	-	0.39	0.33	0.25	0.07	0.05	0.03
1999	0.04	-	0.84	0.73	0.57	0.16	0.11	0.08
2006	0.04	-	-	-	-	-	-	-
2007	0.00	-	-	-	-	-	-	0.03
2023	0.06	-	0.58	0.49	0.37	-	-	0.05
2033	0.00	-	0.39	0.33	0.24	-	-	0.03
2034	0.00	-	-	0.33	0.24	-	-	0.03
2037	0.00	-	0.39	0.33	0.25	-	-	0.03
2058	0.05	1.32	-	0.70	0.54	-	0.10	0.07
2066	0.00	-	0.01	0.02	0.01	-	-	-
2070	0.00	-	0.80	0.70	0.54	0.16	0.11	0.08
2087	0.00	-	0.01	0.01	-	-	-	-
2094	0.00	-	-	-	-	-	-	0.03

Table 8: The output parameters from fitting the SED

VCC (1)	stellar fit (2)	$[F_{6.75}(d+s)/F_{6.75}(s)]$ (3)	c (4)	d (5)
1	S	1.15	-	-
4	-	-	-	-
17	S	3.48	-	-
24	S	0.43	-	-
26	-	-	-	-
66	S	8.53	0.555	-1.536
81	S	-	-	-
87	S	2.77	-	-
92	S	3.63	0.632	-1.555
130	-	-	-	-
152	S	10.10	1.151	-4.827
159	S	-	-	-
169	-	-	-	-
171	-	-	-	-
207	-	-	-	-
318	S	1.68	-	-
425	-	-	-	-
459	T	3.42	-	-
460	S	1.65	0.620	-1.951
655	S	5.31	-	-
664	S	2.29	-	-
666	-	-	-	-
692	S	5.17	-	-
793	S	-	-	-
802	-	-	-	-
809	S	4.23	-	-
836	S	7.30	0.622	-1.141
848	S	1.70	-	-
857	S	1.79	-	-
873	S	12.68	0.847	-2.698
890	-	-	-	-
912	S	3.75	-	-
945	S	-	-	-
950	S	-	-	-
971	S	2.49	-	-
984	S	0.57	-	-
995	S	1.62	-	-
1001	-	-	-	-
1002	S	7.30	1.133	-5.148
1003	S	1.10	-	-
1043	S	1.46	0.569	-0.838
1047	S	-	-	-
1106	-	-	-	-
1110	S	1.06	-	-
1121	-	-	-	-
1158	S	0.69	-	-
1189	S	4.17	-	-
1196	S	0.71	-	-
1200	S	-	-	-
1217	S	1.67	-	-
1253	S	0.74	0.678	-2.555
1257	-	-	-	-
1287	-	-	-	-
1313	S	-	-	-
1326	S	1.66	-	-
1356	S	-	-	-
1368	S	0.58	-	-
1377	S	-	-	-
1379	S	7.41	0.757	-3.368
1403	-	-	-	-
1410	S	5.55	-	-
1411	S	-	-	-
1412	S	0.59	-	-
1419	S	1.55	-	-
1426	S	-	-	-
1448	S	-	-	-
1450	S	11.32	-	-
1486	S	-	-	-
1552	S	1.01	-	-
1554	S	10.18	0.903	-2.677
1569	S	1.58	-	-
1575	S	10.38	-	-
1581	S	-	-	-
1596	-	-	-	-

Table 8: continue

VCC (1)	stellar fit (2)	$[F_{6.75}(d+s)/F_{6.75}(s)]$ (3)	c (4)	d (5)
1644	-	-	-	-
1673	S	6.33	-	-
1675	T	-	-	-
1676	S	8.14	0.671	-1.487
1678	S	-	-	-
1686	S	5.75	-	-
1690	S	3.76	0.461	-0.583
1699	S	2.87	-	-
1725	S	2.07	-	-
1726	S	-	-	-
1727	S	1.91	0.075	1.601
1730	S	2.67	-	-
1750	-	1.78	-	-
1757	S	-	-	-
1758	S	2.94	-	-
1784	-	-	-	-
1789	S	2.49	-	-
1791	S	3.23	-	-
1804	S	1.04	-	-
1811	S	7.28	0.863	-3.643
1813	S	0.80	-	-
1822	S	4.70	-	-
1869	S	-	0.659	-3.058
1885	-	-	-	-
1918	-	5.73	-	-
1929	S	4.60	-	-
1932	S	16.83	0.784	-2.629
1952	-	-	-	-
1970	-	-	-	-
1972	S	12.67	0.962	-3.348
1987	S	11.78	0.659	-1.480
1992	S	3.03	-	-
1999	S	0.51	-	-
2006	-	0.94	-	-
2007	-	4.23	-	-
2023	S	1.83	-	-
2033	S	1.06	-	-
2034	S	0.51	-	-
2037	S	-	-	-
2058	S	4.90	0.675	-2.473
2066	S	3.33	0.044	0.357
2070	S	0.67	0.000	0.301
2087	S	0.44	-	-
2094	-	17.81	-	-

Column 1: VCC name.

Column 2: S indicates galaxies with a fitted Bruzual & Charlot spectrum determined from UV, optical and near-IR spectro-photometry, T for galaxies whose fit is Bruzual & Charlot spectrum of the template.

Column 3: The ratio of the total flux (star plus dust) to the stellar flux at 6.75 μm, $[F_{6.75}(d+s)/F_{6.75}(s)]$.

Column 4 and 5: the fit of the radio continuum data, where a and b are the slope and the intercept of the relation $logF(\nu) = c \times log\lambda + d$, with ν in Hz and λ in μm. Given the inconsistency in their radio continuum flux densities, the fitting coefficients of the galaxies VCC 857, 1110 and 1450 are not given.

Table 9: Template dust extinction corrected SEDs

λ (μm)	$Log(F(\nu)/F(K))$											
	S0a	Sa	Sab-Sb	Sbc-Sc	Scd-Sd	Im	BCD	L_H<8.3	8.3≤L_H<9	9≤L_H<9.8	9.8≤L_H<10.5	L_H≥10.5
0.20	-3.22(2)	-2.46(5)	-1.51(5)	-1.04(15)	-0.72(4)	-0.38(7)	-0.36(4)	− (1)	-0.37(11)	-0.87(9)	-1.22(12)	-1.62(10)
0.37	-1.25(5)	-0.96(10)	-0.92(7)	-0.59(16)	-0.47(6)	-0.26(15)	-0.32(9)	-0.12(3)	-0.28(21)	-0.58(17)	-0.88(15)	-1.06(16)
0.44	-0.78(6)	-0.42(11)	-0.45(7)	-0.26(22)	-0.16(6)	0.06(21)	-0.10(11)	0.11(4)	-0.03(27)	-0.21(21)	-0.40(19)	-0.53(18)
0.55	-0.48(6)	-0.21(11)	-0.25(7)	-0.13(22)	-0.07(6)	0.13(21)	-0.04(10)	0.23(3)	0.08(27)	-0.09(21)	-0.18(19)	-0.28(18)
1.25	0.06(5)	0.07(9)	0.05(6)	-0.02(7)	−(−)	0.19(6)	0.08(2)	0.22(2)	0.19(4)	0.09(3)	0.05(12)	0.06(16)
1.65	0.13(6)	0.13(10)	0.11(6)	0.13(14)	−(1)	0.15(7)	0.11(2)	0.21(2)	0.15(5)	0.14(7)	0.13(19)	0.12(16)
2.10	0.00(6)	0.00(11)	0.00(7)	0.00(22)	0.00(6)	0.00(35)	0.00(17)	0.00(20)	0.00(32)	0.00(22)	0.00(19)	0.00(18)
6.75	-0.95(5)	-0.96(9)	-0.46(7)	-0.14(21)	-0.37(5)	-0.19(14)	-0.57(11)	-0.15(4)	-0.35(18)	-0.34(18)	-0.16(18)	-0.61(17)
12	−(1)	-0.54(4)	-0.24(7)	0.26(13)	−(1)	−(1)	−(-)	− (-)	− (-)	− (1)	0.13(13)	-0.33(14)
15	-1.37(5)	-1.30(10)	-0.47(7)	-0.13(21)	-0.14(4)	0.06(9)	-0.48(7)	0.02(2)	-0.30(10)	-0.46(18)	-0.22(19)	-0.63(17)
25	−(1)	−(1)	-0.40(7)	0.46(13)	−(1)	−(1)	−(1)	− (-)	− (1)	0.72(3)	0.28(11)	-0.10(12)
60	-0.19(2)	0.19(7)	0.43(7)	1.14(17)	1.29(5)	1.44(6)	1.39(6)	− (-)	1.48(10)	1.18(14)	1.05(14)	0.43(15)
100	0.36(2)	1.01(6)	0.97(7)	1.63(17)	1.72(5)	1.78(7)	1.65(8)	2.00(3)	1.70(9)	1.67(14)	1.61(13)	0.97(15)
170	0.36(4)	1.15(5)	1.27(7)	1.78(11)	1.88(4)	1.89(10)	1.93(9)	2.05(4)	1.82(12)	1.83(15)	1.68(10)	1.15(11)
28000	−(1)	−(1)	-1.55(5)	-1.46(8)	−(−)	−(1)	−(-)	− (-)	− (-)	− (-)	-1.63(9)	-1.44(9)
63000	-2.46(2)	-2.09(2)	-1.57(5)	-1.08(11)	−(−)	−(1)	−(-)	− (-)	− (-)	− (1)	-1.21(9)	-1.40(12)
126000	-2.00(3)	-1.68(6)	-1.34(5)	-1.01(10)	−(1)	−(1)	−(1)	− (-)	− (-)	− (1)	-1.10(13)	-1.47(14)
210000	−(1)	−(1)	-1.31(5)	-0.81(10)	-0.72(2)	0.33(4)	−(1)	− (-)	0.51(3)	-0.72(3)	-0.95(11)	-1.06(10)

Note: the values in parenthesis give the total number of objects in each Hubble type and wavelength bin that were combined to form the templates

Table 10: Example of Template dust extinction corrected B&C SEDs

λ (μm)	$Log(F(\nu)/F(K))$											
	S0a	Sa	Sab-Sb	Sbc-Sc	Scd-Sd	Im	BCD	L_H<8.3	8.3≤L_H<9	9≤L_H<9.8	9.8≤L_H<10.5	L_H≥10.5
0.1005	-3.26	-2.88	-2.04	-1.03	-0.81	-0.58	-0.40	-0.36	-0.51	-0.97	-1.26	-2.08
0.1015	-3.25	-2.88	-2.06	-1.05	-0.83	-0.62	-0.44	-0.40	-0.55	-1.01	-1.25	-2.09
0.1025	-3.36	-3.02	-2.25	-1.28	-1.02	-0.85	-0.67	-0.63	-0.77	-1.24	-1.42	-2.28
0.1035	-3.28	-2.91	-2.10	-1.09	-0.87	-0.65	-0.46	-0.43	-0.57	-1.04	-1.30	-2.13
0.1045	-3.19	-2.83	-1.98	-0.98	-0.75	-0.55	-0.37	-0.34	-0.48	-0.95	-1.16	-2.02
0.1055	-3.20	-2.83	-1.98	-0.97	-0.75	-0.54	-0.36	-0.32	-0.47	-0.93	-1.17	-2.01
...	...	...	...	...	...	...	...	...	...	...	...	...
1.0025	-0.02	0.14	0.08	0.08	0.15	0.05	0.22	0.32	0.18	0.12	0.11	0.06
1.0075	-0.02	0.13	0.07	0.08	0.15	0.04	0.21	0.32	0.17	0.12	0.10	0.05
1.0125	-0.02	0.14	0.08	0.08	0.15	0.05	0.22	0.33	0.18	0.12	0.11	0.06
1.0175	-0.02	0.14	0.08	0.08	0.15	0.05	0.22	0.32	0.18	0.12	0.10	0.06
1.0225	-0.01	0.14	0.08	0.08	0.15	0.05	0.22	0.32	0.18	0.12	0.11	0.06
...	...	...	...	...	...	...	...	...	...	...	...	...
9.7800	-1.09	-1.05	-1.10	-1.09	-1.02	-1.24	-1.06	-0.96	-1.10	-1.06	-1.07	-1.10
9.8200	-1.09	-1.05	-1.10	-1.09	-1.02	-1.24	-1.07	-0.96	-1.11	-1.06	-1.07	-1.11
9.8600	-1.09	-1.05	-1.11	-1.09	-1.02	-1.24	-1.07	-0.96	-1.11	-1.07	-1.07	-1.11
9.9000	-1.10	-1.05	-1.11	-1.09	-1.02	-1.24	-1.07	-0.96	-1.11	-1.07	-1.07	-1.11
9.9400	-1.10	-1.06	-1.11	-1.10	-1.03	-1.25	-1.08	-0.97	-1.12	-1.07	-1.08	-1.11
9.9800	-1.10	-1.06	-1.12	-1.11	-1.03	-1.25	-1.08	-0.97	-1.12	-1.08	-1.08	-1.12
10.0200	-1.11	-1.07	-1.12	-1.11	-1.04	-1.26	-1.09	-0.98	-1.12	-1.08	-1.09	-1.12

Notes: Table 10, 11 (template dust extinction uncorrected) and 12 (template FIR fit) are available only in electronic format at http://cdsweb.u-strasbg.fr